Electronic Supplementary Information (ESI)

Labile Coordination Approach for Modulation of Electronic Properties in Ruthenium(II) and Iridium(III) Complexes within "N-Heterocyclic Carbene (NHC)–Pyridyl" Dynamic Platform

Moumita Mondal[§], Ranjeesh T. K.[§], Suraj K. Gupta, and Joyanta Choudhury*

Department of Chemistry, Indian Institute of Science Education and Research Bhopal, Bhopal 462 023, India
**Corresponding Author: joyanta@iiserb.ac.in*

§ These authors contributed equally.

Table of Contents

I. ^{1}H NMR, ^{13}C{^{1}H} NMR, and ESI-MS spectra of 1, 2, 3, 4, 5, 6, 7:

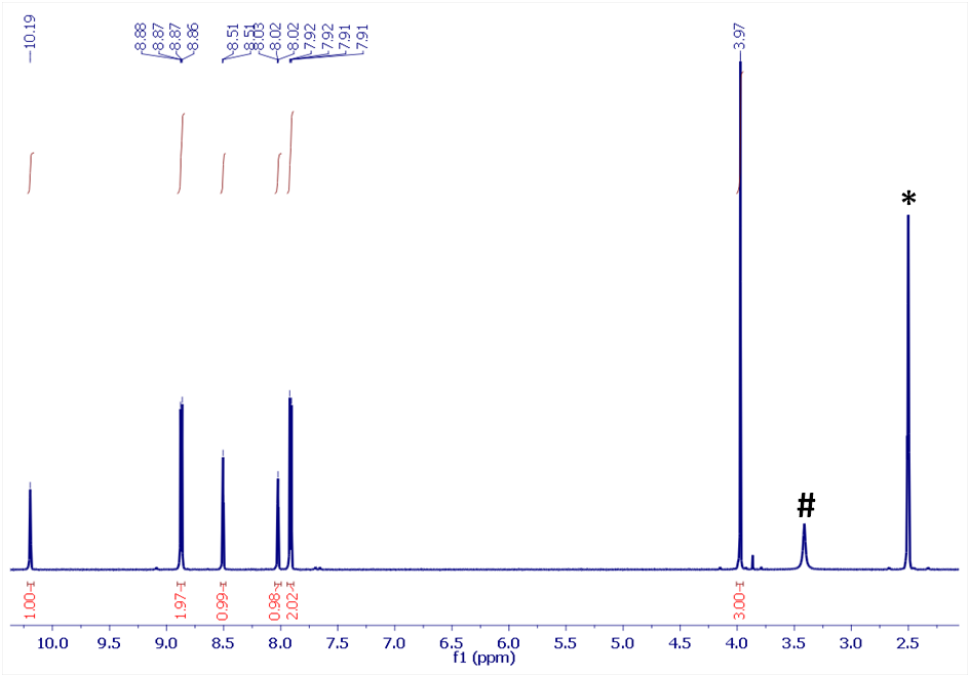

Figure S1 ^{1}H NMR spectrum of **1** (400 MHz, [D_6]DMSO, 300 K).

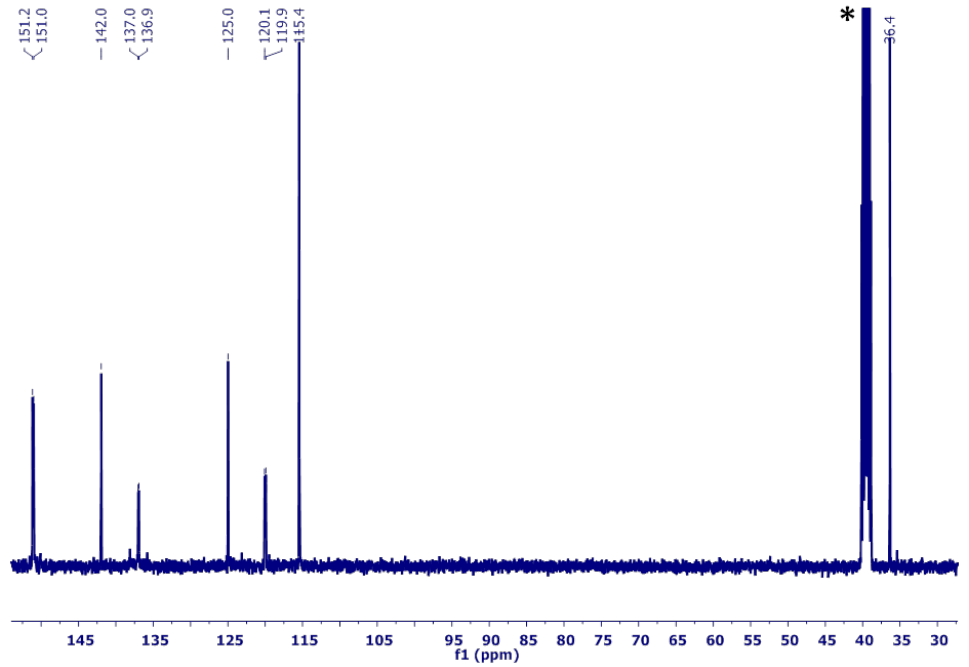

Figure S2 ^{13}C NMR spectrum of **1** (100 MHz, [D_6]DMSO, 300 K).

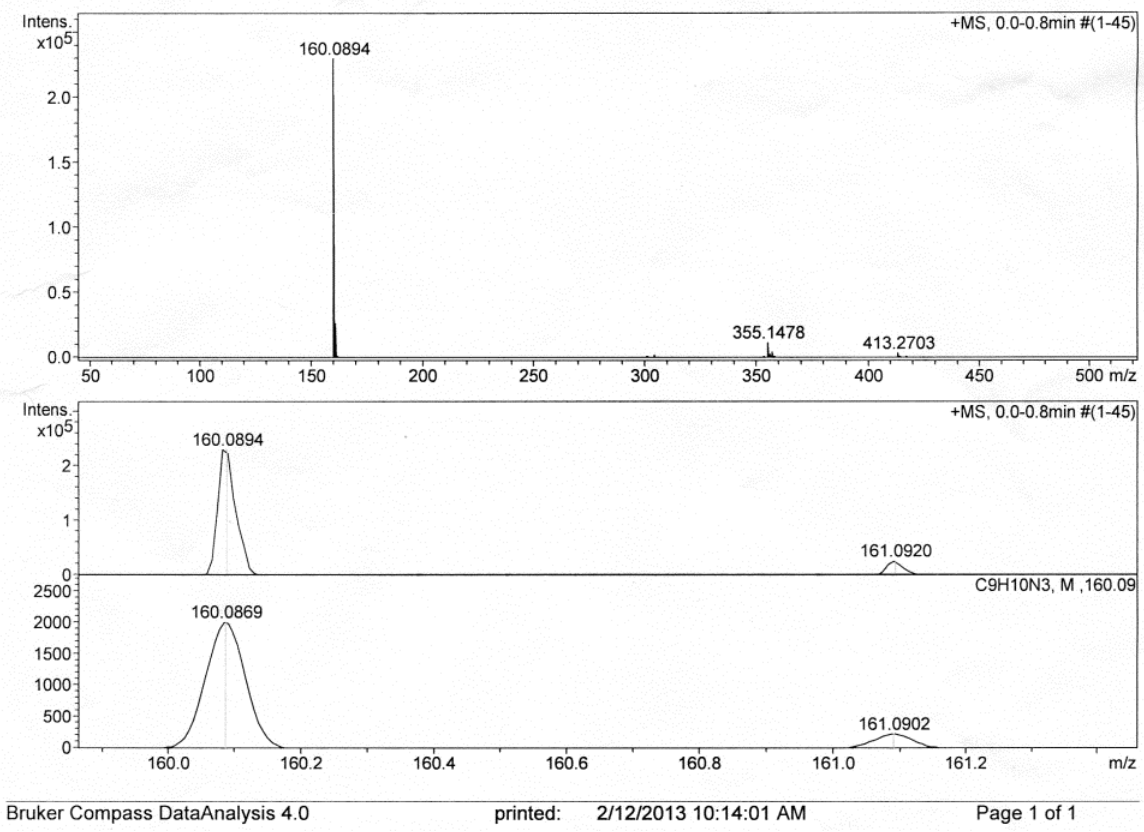

Figure S3 ESI-MS (positive ion mode) spectrum of **1**.

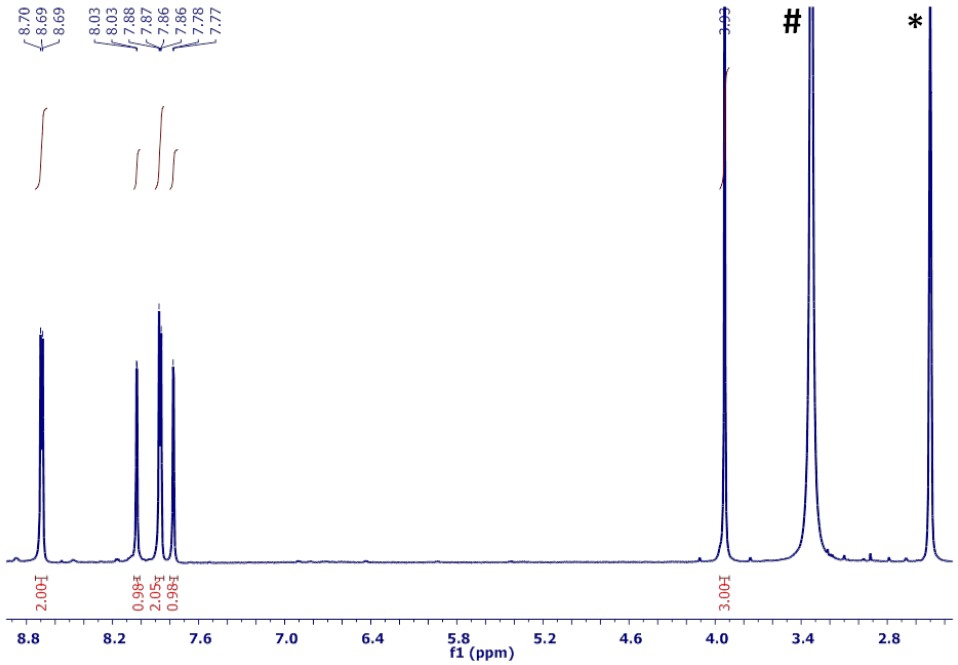

Figure S4 ^{1}H NMR spectrum of **2** (400 MHz, [D_6]DMSO, 300 K).

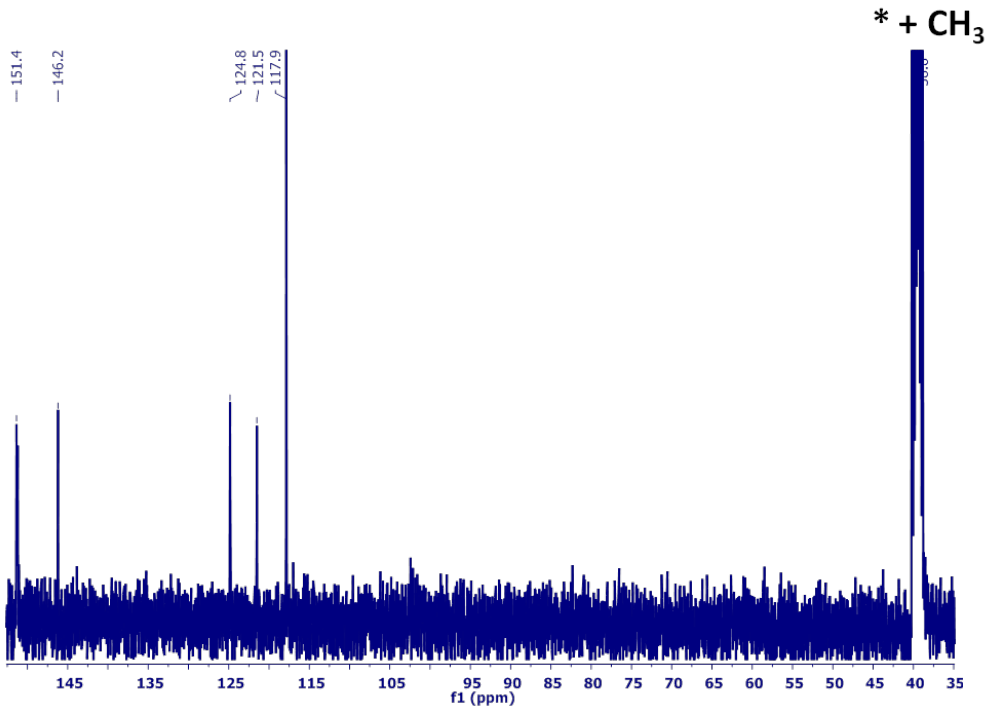

Figure S5 ^{13}C NMR spectrum of **2** (100 MHz, [D_6]DMSO, 300 K).

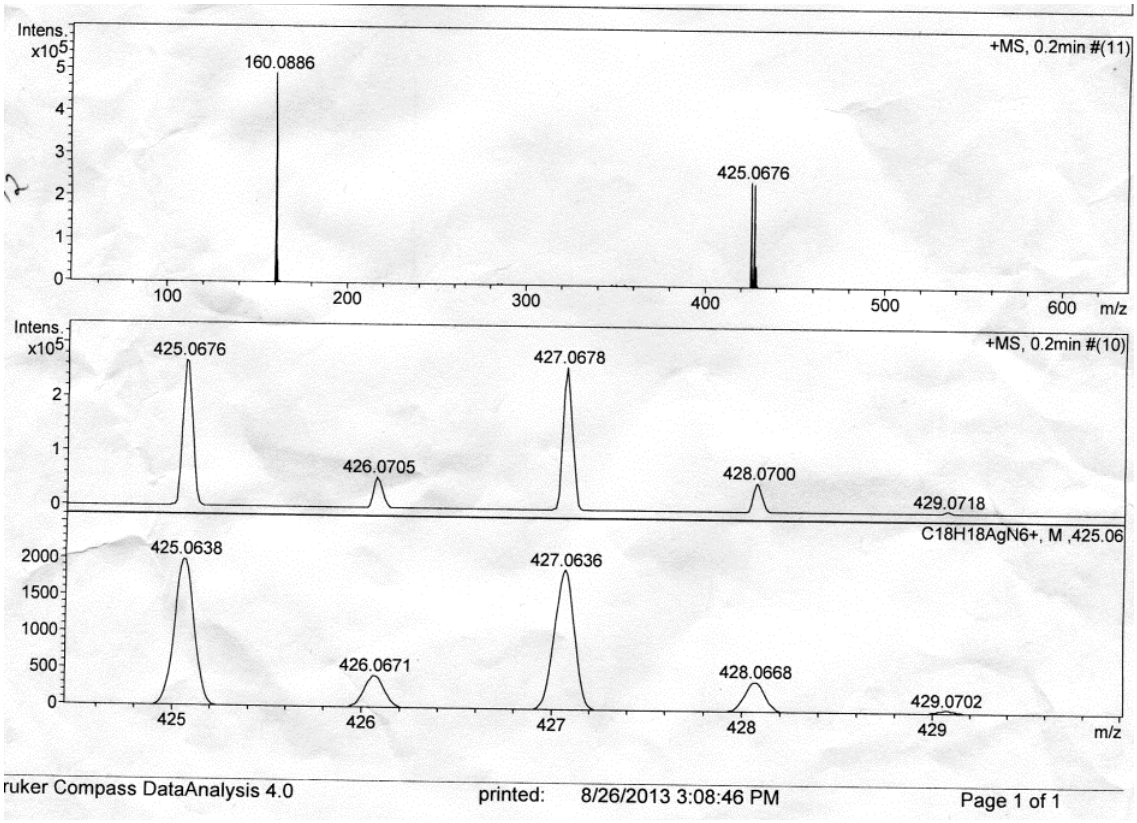

Figure S6 ESI-MS (positive ion mode) spectrum of **2**.

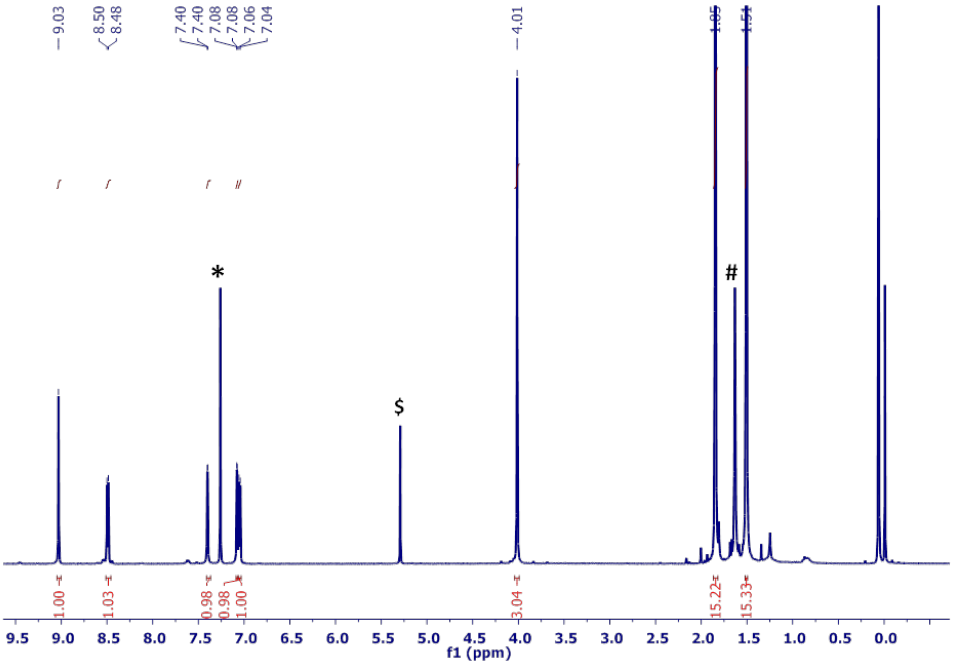

Figure S7 ^{1}H NMR spectrum of **3** (400 MHz, $CDCl_3$, 300 K).

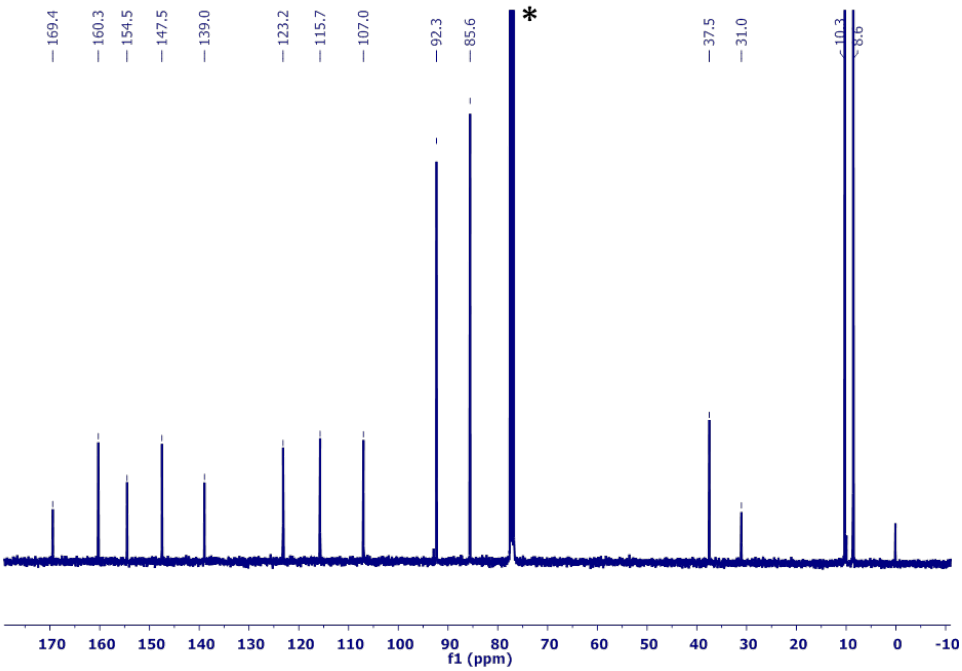

Figure S8 ^{13}C NMR spectrum of **3** (100 MHz, $CDCl_3$, 300 K).

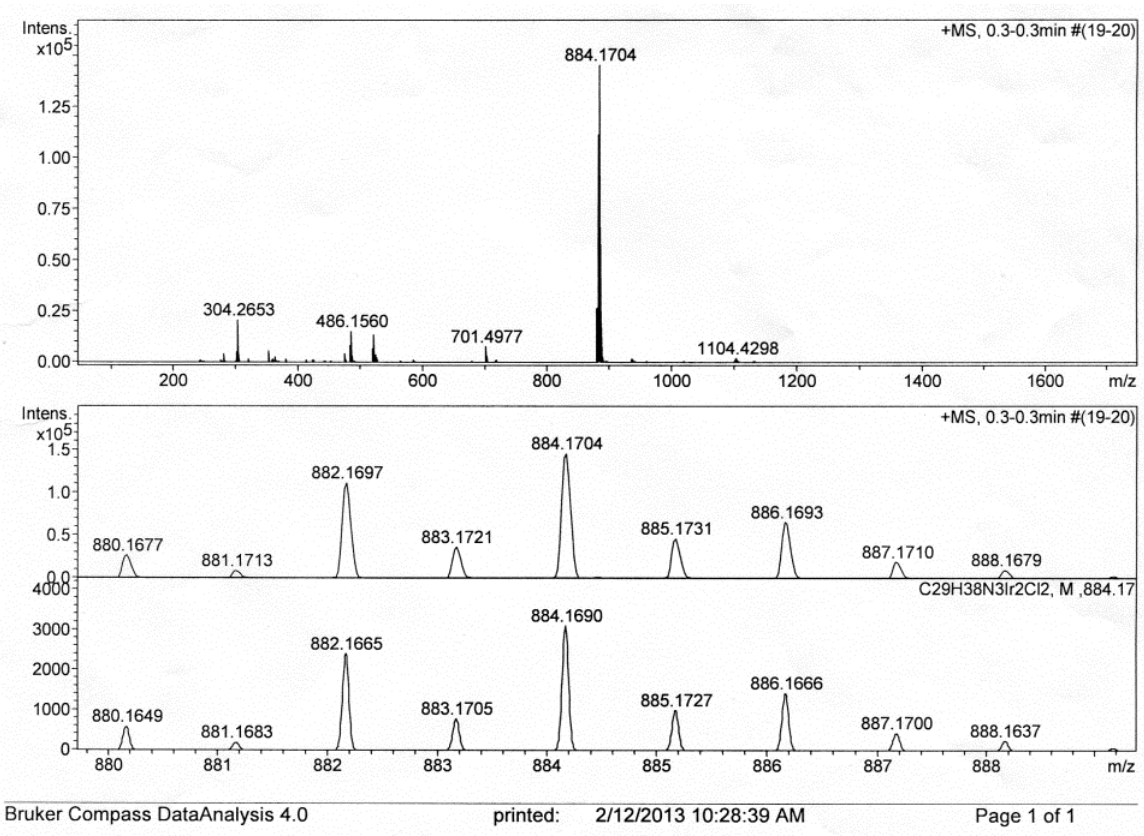

Figure S9 ESI-MS (positive ion mode) spectrum of **3**.

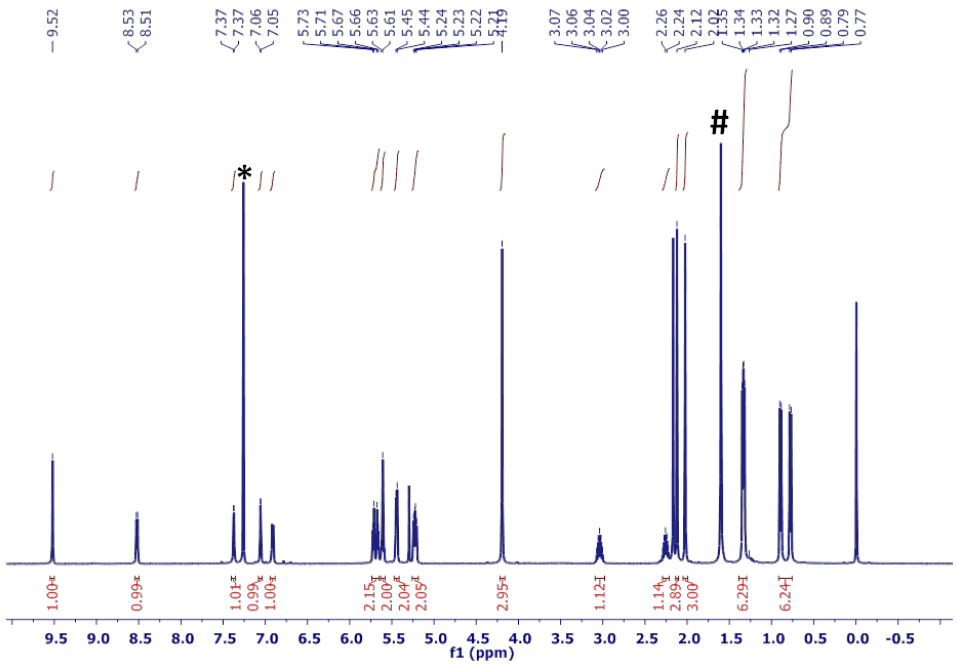

Figure S10 ^{1}H NMR spectrum of **4** (400 MHz, $CDCl_3$, 300 K).

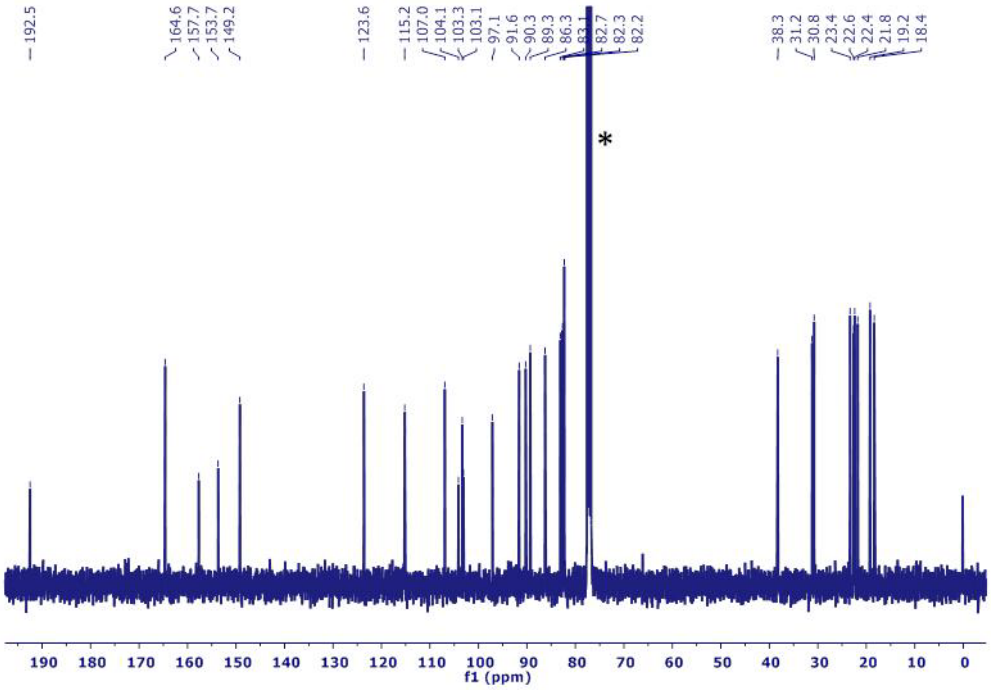

Figure S11 ^{13}C NMR spectrum of **4** (100 MHz, $CDCl_3$, 300 K).

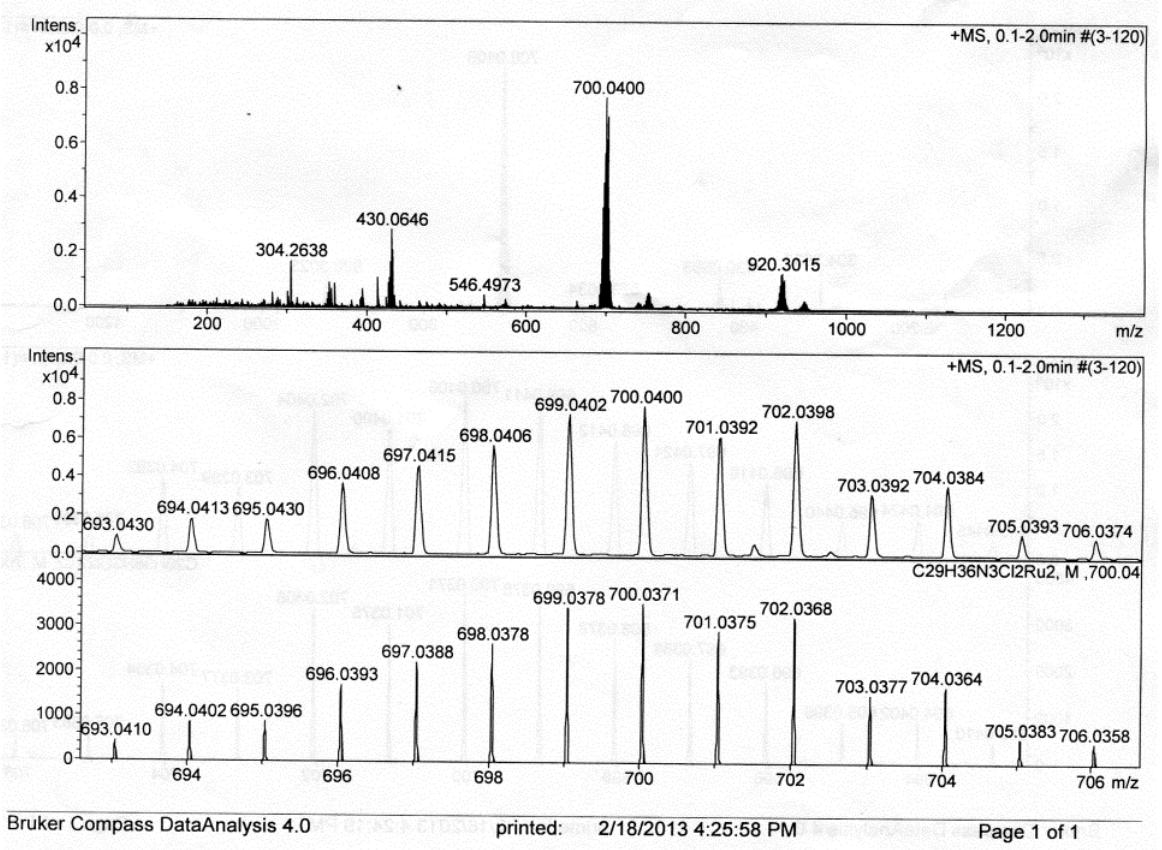

Figure S12 ESI-MS (positive ion mode) spectrum of **4**.

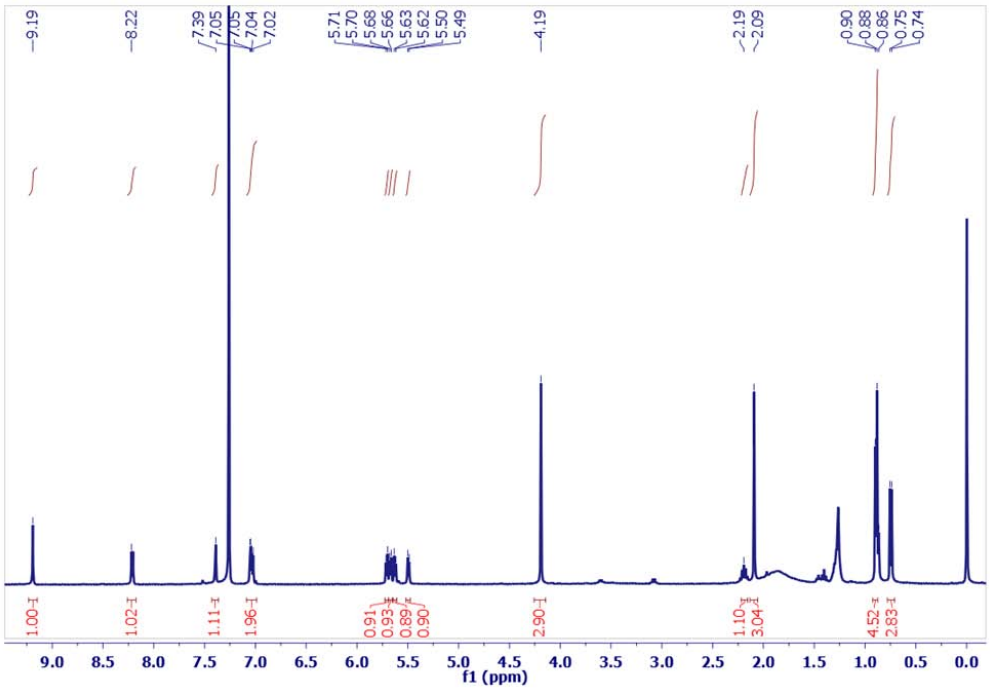

Figure S13 ^{1}H NMR spectrum of **5** (400 MHz, $CDCl_3$, 300 K).

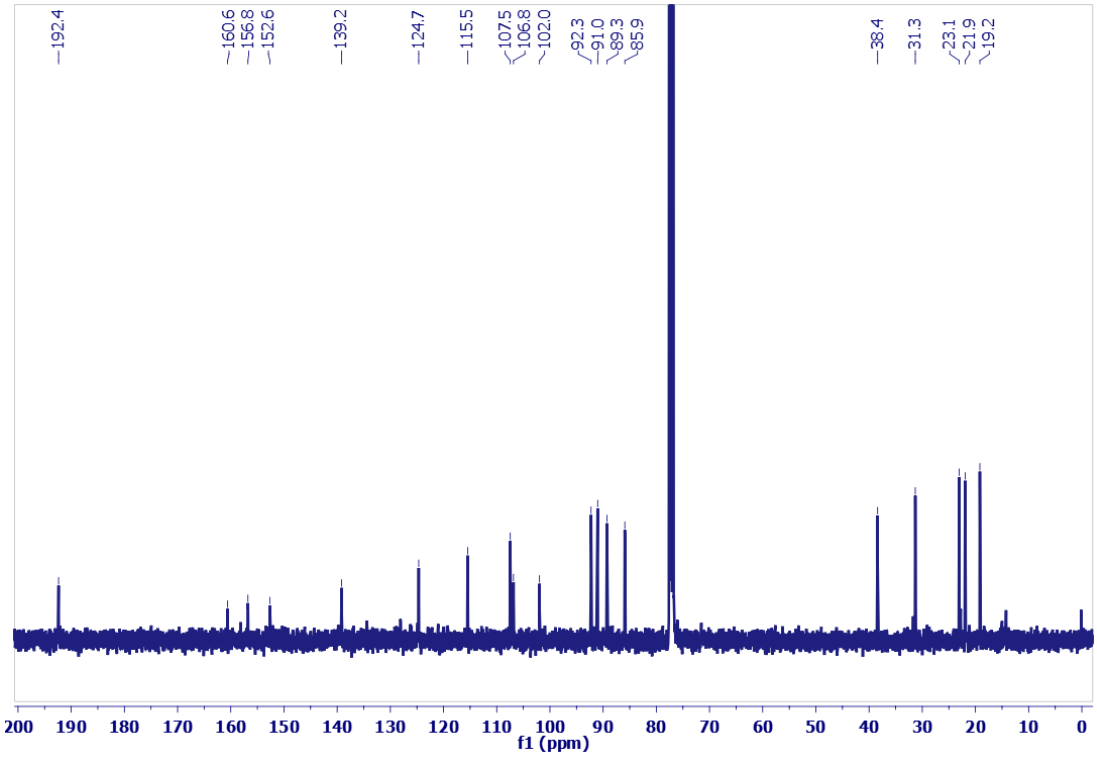

Figure S14 ^{13}C NMR spectrum of **5** (100 MHz, $CDCl_3$, 300 K).

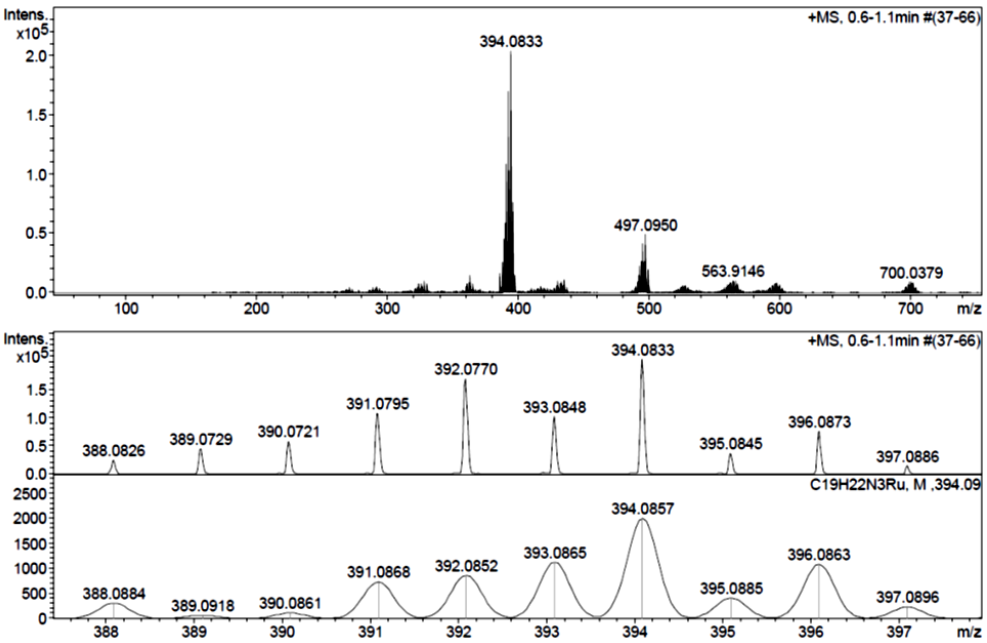

Figure S15 ESI-MS (positive ion mode) spectrum of **5**.

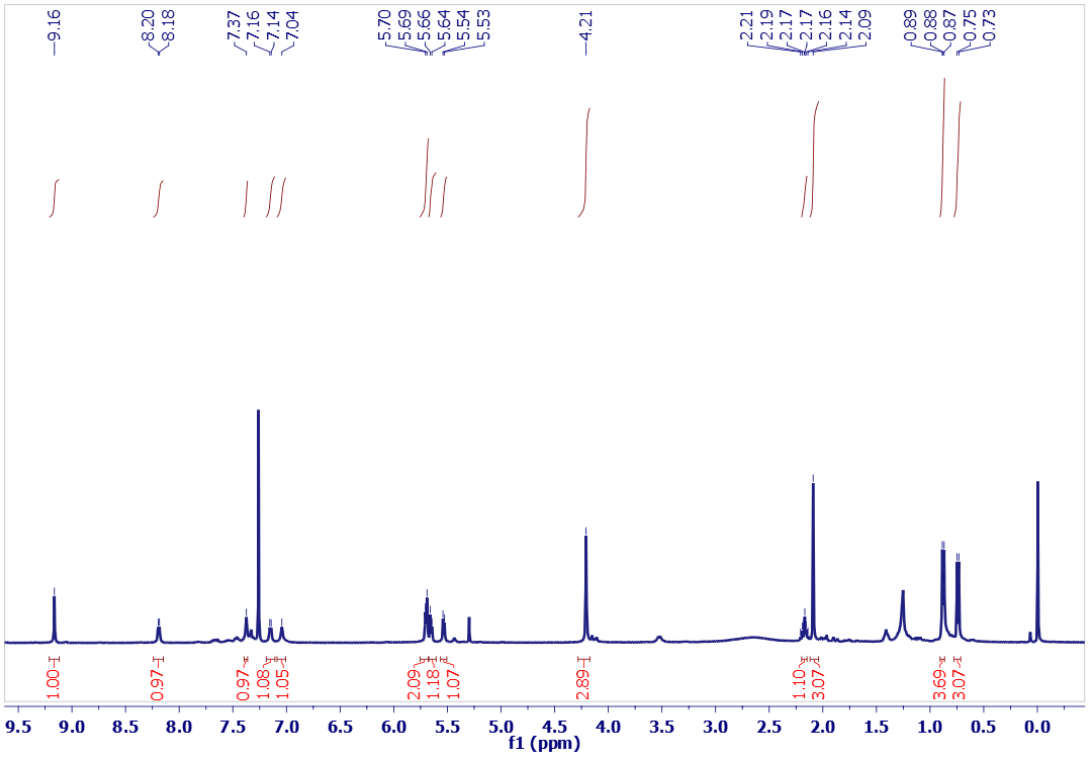

Figure S16 ^{1}H NMR spectrum of **6** (400 MHz, $CDCl_3$, 300 K).

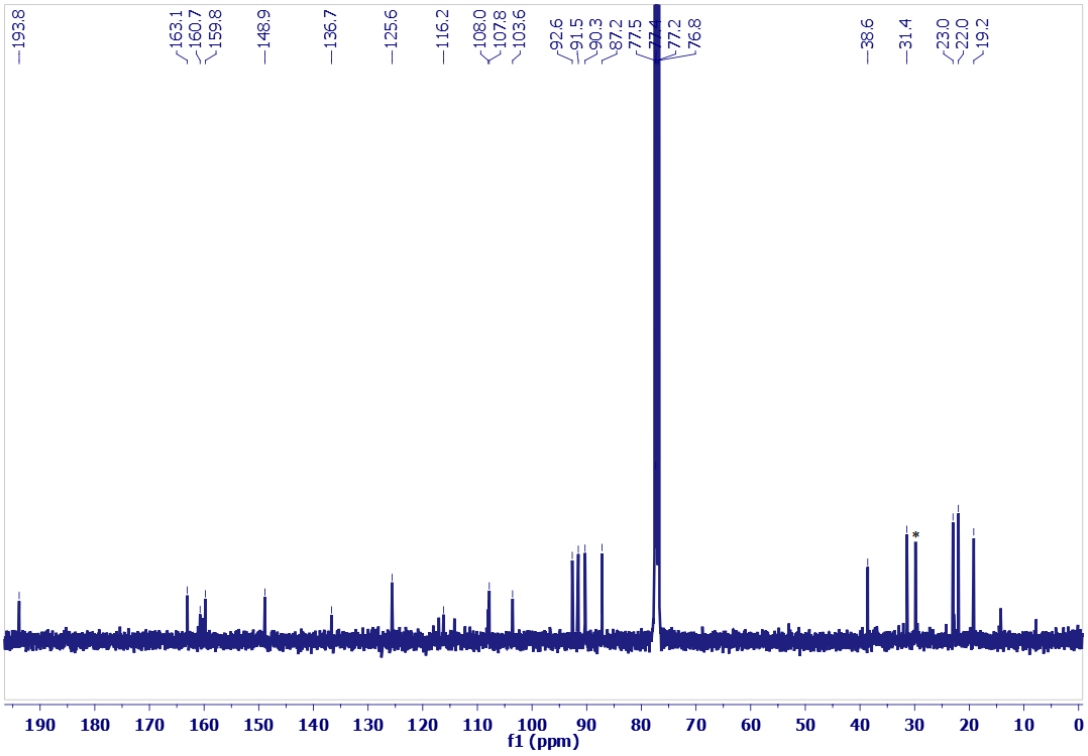

Figure S17 ^{13}C NMR spectrum of **6** (100 MHz, $CDCl_3$, 300 K).

*(*an unwanted peak due to some unknown impurity)*

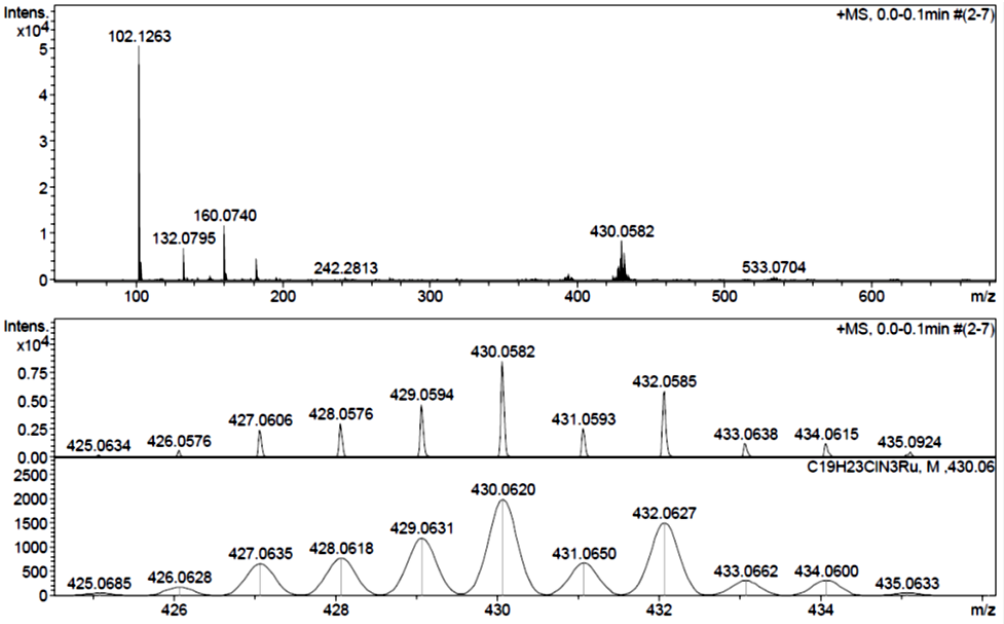

Figure S18 ESI-MS (positive ion mode) spectrum of **6**.

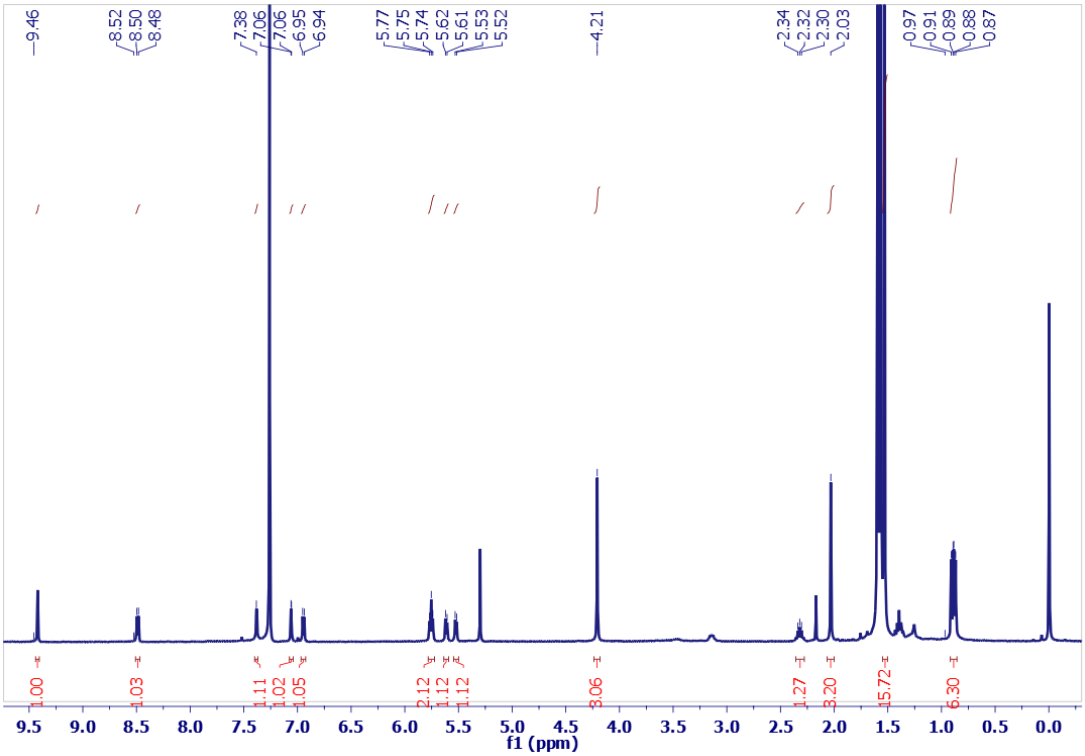

Figure S19 ^{1}H NMR spectrum of **7** (400 MHz, $CDCl_3$, 300 K).

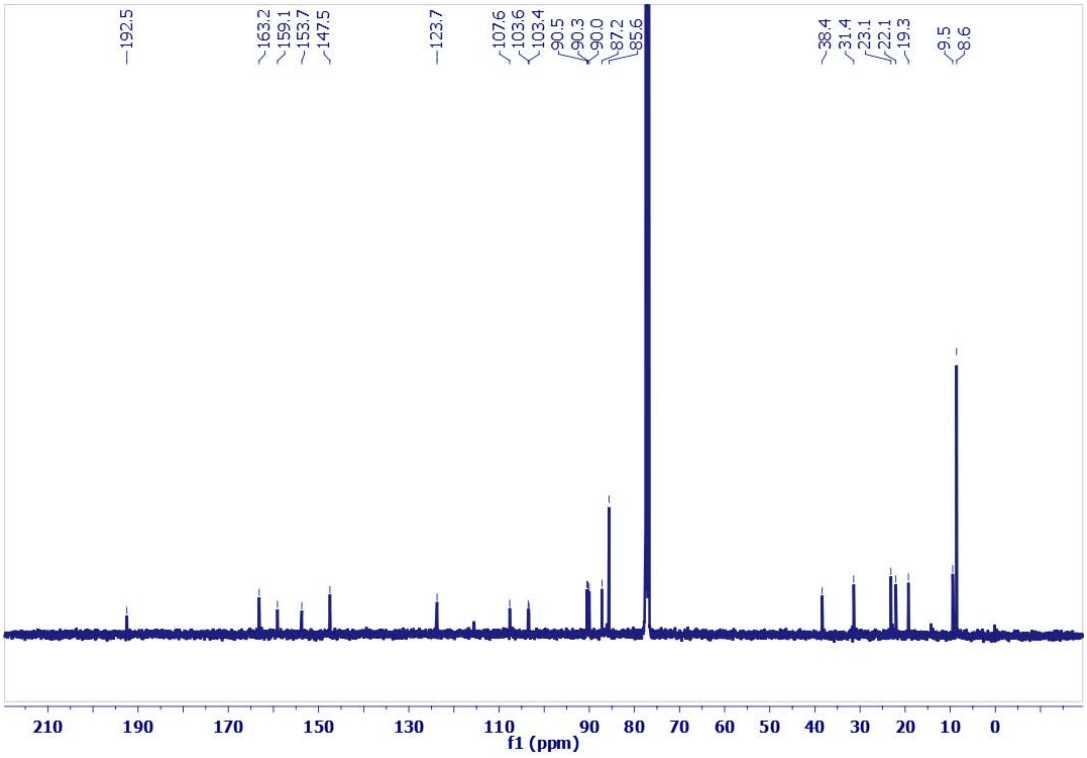

Figure S20 ^{13}C NMR spectrum of **7** (100 MHz, $CDCl_3$, 300 K).

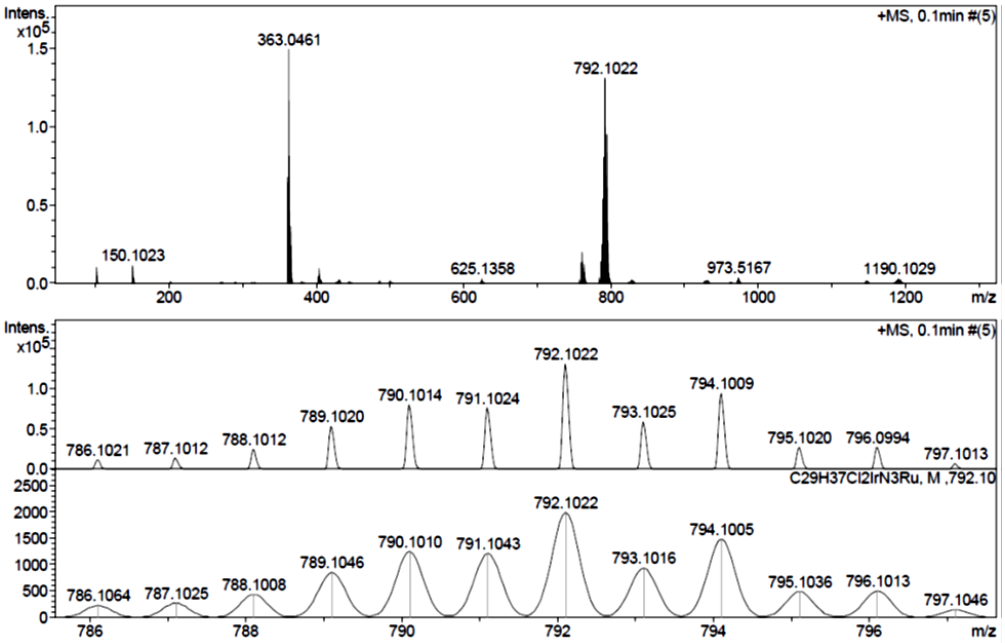

Figure S21 ESI-MS (positive ion mode) spectrum of **7**.

II. Stimuli-responsive studies:

(A) Reversible decoordination–recoordination switching experiments:

(i) Decoordination:

Reaction of 3 with PPh_3: 3 (2.9 mg, 3.15 μmol) was dissolved in $CDCl_3$ (0.3 mL) in an NMR tube and PPh_3 (31 μL, 0.10 M solution in $CDCl_3$, ~3.15 μmol) was added to it. The tube was shaken for few minutes and kept for 3 h at room temperature. The reaction mixture was monitored by ^{1}H NMR spectroscopy for completion of the reaction and generation of the decoordinated complex (*vide* Table S1 and Figure S22). The simultaneous formation of $IrCp^*Cl_2(PPh_3)$ was confirmed by comparison with reported ^{1}H NMR chemical shift values [S1].

Reaction of 4 with PPh_3: 4 (2.2 mg, 2.97 μmol) was dissolved in $CDCl_3$ (0.3 mL) in an NMR tube and PPh_3 (29 μL, 0.16 M solution in $CDCl_3$, ~4.45 μmol) was added to it. The tube was shaken for few minutes and kept for 3 h at room temperature. The reaction mixture was monitored by ^{1}H NMR spectroscopy for completion of the reaction and generation of the decoordinated complex (*vide* Table S2 and Figure S23). The simultaneous formation of Ru(*p*-cym)$Cl_2(PPh_3)$ was confirmed by comparison with reported ^{1}H NMR chemical shift values [S2].

(ii) Recoordination:

Regeneration of 3: 3 (2.7 mg, 2.94 μmol) was dissolved in $CDCl_3$ (0.3 mL) in an NMR tube and PPh_3 (24 μL, 0.12 M solution in $CDCl_3$, ~2.94 μmol) was added to it. The tube was shaken for few minutes and kept for 3 h at room temperature. After confirming the complete generation of the decoordinated complex (by ^{1}H NMR spectral monitoring), $[IrCp^*Cl_2]_2$ (28 μL, 0.05 M solution in $CDCl_3$, ~1.47 μmol) was added to the same reaction mixture. Complete regeneration of **3** was achieved after 1 h as confirmed by ^{1}H NMR spectroscopic analysis (*vide* Table S1 and Figure S22).

Regeneration of 4: 4 (3 mg, 4.06 μmol) was dissolved in $CDCl_3$ (0.3 mL) in an NMR tube and PPh_3 (41 μL, 0.16 M solution in $CDCl_3$, ~6.09 μmol) was added to the solution. The tube was shaken for few minutes and kept for 3 h at room temperature. After confirming the complete generation of the decoordinated complex (by ^{1}H NMR spectral monitoring), [Ru(*p*-cym)$Cl_2]_2$ (97μL, 0.02 M solution in $CDCl_3$, ~2.03 μmol) was added to the same reaction mixture. Complete regeneration of **4** was achieved after 1 h as confirmed by ^{1}H NMR spectroscopic analysis (*vide* Table S2 and Figure S23).

(iii) Coordination with different metal center:

Reaction of the iridium complex with [Ru(*p*-cym)$Cl_2]_2$: 3 (2.3 mg, 2.50 μmol) was dissolved in $CDCl_3$ (0.3 mL) in an NMR tube and PPh_3 (17 μL, 0.14 M solution in $CDCl_3$, ~2.50 μmol) was added to it. The tube was shaken for few minutes and kept for 3 h at room temperature. After confirming the complete generation of the decoordinated complex (by ^{1}H NMR spectral monitoring), [([Ru(*p*-cym)$Cl_2]_2$ (35 μL, 0.03 M solution in $CDCl_3$, ~1.25 μmol) was added to the reaction mixture and monitored again for completion of the reaction. Complete generation of the heterobimetallic complex

was achieved after 1 h as confirmed by ^{1}H NMR spectroscopic analysis (*vide* Table S1 and Figure S22). *Note: A competitive formation of Ru(p-cym)$Cl_2(PPh_3)$ was traced by characteristic ^{1}H NMR chemical shifts which could possibly be generated by the reversible reaction between IrCp*$Cl_2(PPh_3)$ and $[(p\text{-cym})RuCl_2]_2$.*

Reaction of the ruthenium complex with $[IrCp^*Cl_2]_2$: 4 (2.2 mg, 2.97 μmol) was dissolved in $CDCl_3$ (0.3 mL) in an NMR tube and PPh_3 (29μL, 0.16 M solution in $CDCl_3$, ~4.45 μmol) was added to the solution. The NMR tube was shaken for few minutes and kept for 3 h at room temperature. After confirming the complete generation of the decoordinated complex (by ^{1}H NMR spectral monitoring), $[IrCp^*Cl_2]_2$ (164 μL, 0.018 M solution in $CDCl_3$, ~2.97 μmol) was added to the reaction mixture and monitored again for completion of the reaction. Complete generation of the heterobimetallic complex was achieved after 1 h as confirmed by ^{1}H NMR spectroscopic analysis (*vide* Table S2 and Figure S23). *Note: A competitive formation of IrCp*$Cl_2(PPh_3)$ was traced by characteristic ^{1}H NMR chemical shifts which could possibly be generated by the reversible reaction between Ru(p-cym)$Cl_2(PPh_3)$ and $[IrCp^*Cl_2]_2$.*

(B) Reversible protonation–deprotonation switching experiments:

(i) Experiment with decoordinated iridium complex:

3 (2.9 mg, 3.15 μmol) was dissolved in $CDCl_3$ (0.3 mL) in an NMR tube and PPh_3 (31 μL, 0.10 M solution in $CDCl_3$, ~3.15 μmol) was added to it. The tube was shaken for few minutes and kept for 3 h. After confirming the complete generation of the decoordinated complex (by ^{1}H NMR spectral monitoring), equivalent amount of CF_3COOH (25 μL, 0.13 M solution in $CDCl_3$, ~3.15 μmol) was added to the same reaction mixture and monitored again by ^{1}H NMR spectroscopy for completion of the protonation reaction and generation of the protonated complex after 1 h. To the above solution containing the protonated complex, equivalent amount of NEt_3 (44 μL, 0.07 M solution in $CDCl_3$, ~3.15 μmol) was added and monitored by ^{1}H NMR spectroscopy for completion of deprotonation and regeneration of the deprotonated (or decoordinated) complex after 1 h. The study was repeated for the second time and the results were found to be reproducible (*vide* Table S1 and Figure S22).

(ii) Experiment with decoordinated ruthenium complex:

4 (2.2 mg, 2.97 μmol) was dissolved in $CDCl_3$ (0.3 mL) in an NMR tube and PPh_3 (29 μL, 0.16 M solution in $CDCl_3$, ~4.45 μmol) was added to the solution. The NMR tube was shaken for few minutes and kept for 3 h. After confirming the complete generation of the decoordinated complex (by ^{1}H NMR spectral monitoring), equivalent amount of CF_3COOH (24 μL, 0.13 M solution in $CDCl_3$, ~2.97 μmol) was added to the same reaction mixture and monitored again by ^{1}H NMR spectroscopy for completion of the protonation reaction and generation of the protonated complex after 1 h. To the above solution containing the protonated complex, equivalent amount of NEt_3 (22 μL, 0.14 M solution in $CDCl_3$,

~2.97 μmol) was added and monitored by ^{1}H NMR spectroscopy for completion of deprotonation and regeneration of the deprotonated (or decoordinated) complex after 1 h. The study was repeated for the second time and the results were found to be reproducible (*vide* Table S2 and Figure S23).

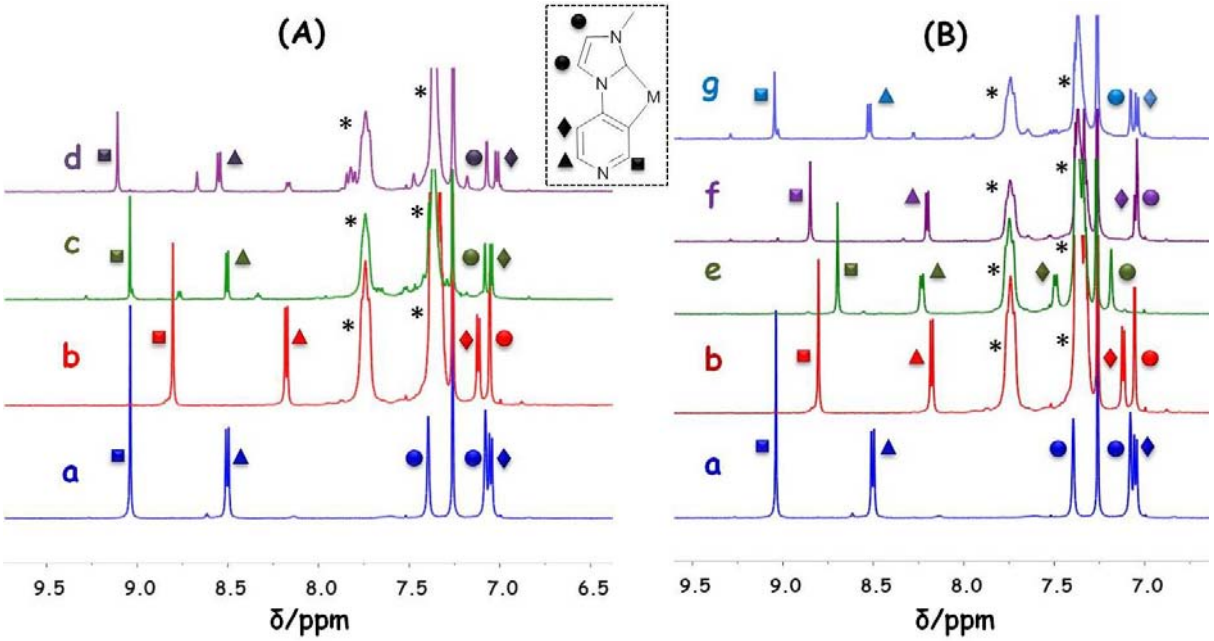

Figure S22 Partial ^{1}H NMR spectra (400 MHz, $CDCl_3$, 300 K) for in situ stimuli-controlled reversible decoordination–recoordination **(A)** and protonation–deprotonation **(B)** switching processes demonstrated with [ClCp*Ir^{III}(μ-PyIm)Ir^{III}Cp*Cl_2], **(3)** (*vide* Scheme 2). **(A)**: **(a) 3** (starting); **(b) 3** + PPh_3; **(c)** regenerated **3** (*via* **3** + PPh_3 + $[IrCp^*Cl_2]_2$); **(d) 3** + PPh_3 + $[Ru(p\text{-cym})Cl_2]_2$). **(B)**: **(a)** complex **3** (starting); **(b) 3** + PPh_3; **(e) 3** + PPh_3 + CF_3COOH; **(f) 3** + PPh_3 + CF_3COOH + NEt_3; **(g)** regenerated **3** (*via* **3** + PPh_3 + CF_3COOH + NEt_3 + $[IrCp^*Cl_2]_2$). Residual solvent peak at δ = 7.26 ppm in $CDCl_3$ was taken as reference for all the spectra. The relevant protons in the complex backbone have been labelled (as■, ▲, ♦, and ● on the structure) and shown in the figure. Asterisks (*) indicate the PPh_3 resonances. Generation of the decoordinated/recoordinated and protonated/deprotonated species was confirmed by recording ESI-HRMS data in solution (***see section IV***).

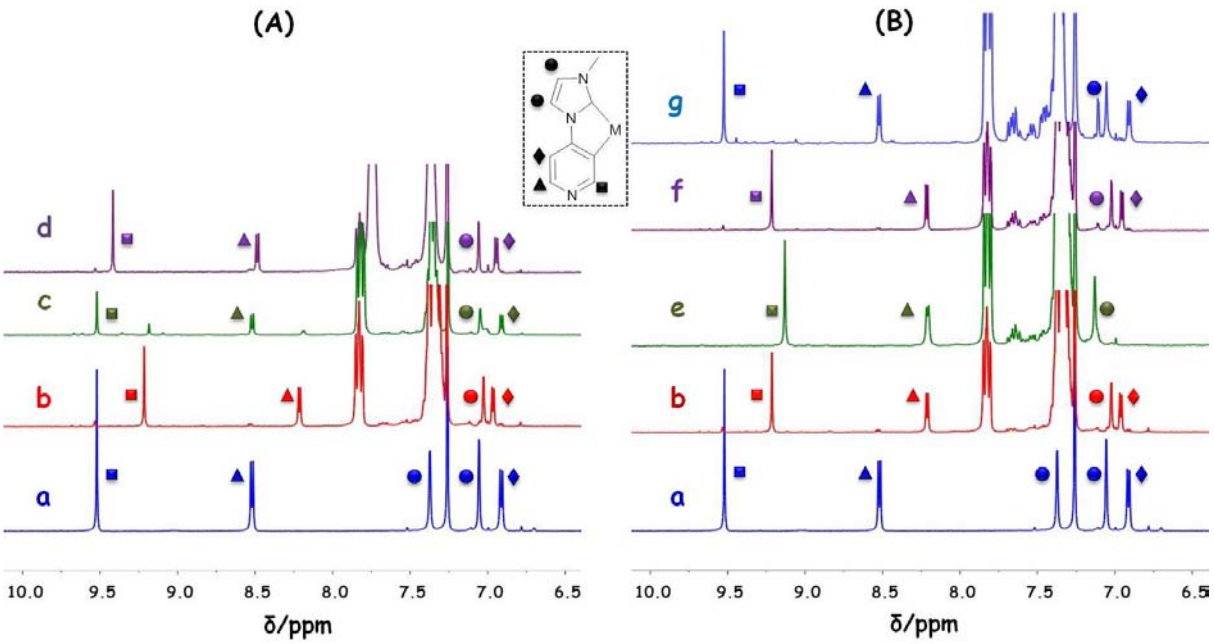

Figure S23 Partial ^{1}H NMR spectra (400 MHz, $CDCl_3$, 300 K) for stimuli-controlled reversible decoordination–recoordination **(A)** and protonation–deprotonation **(B)** switching processes demonstrated with [Cl(*p*-cym)Ru^{II}(μ-PyIm)Ru^{II}(*p*-cym)Cl_2], (**4**) (*vide* Scheme 2). **(A)**: **(a) 4** (starting); **(b) 4** + PPh_3; **(c)** regenerated **4** (via **4** + PPh_3 + [Ru(*p*-cym)Cl_2]$_2$); **(d) 4** + PPh_3 + [IrCp*Cl_2]$_2$. **(B)**: **(a)** complex **4** (starting); **(b) 4** + PPh_3; **(e) 4** + PPh_3 + CF_3COOH; **(f) 4** + PPh_3 + CF_3COOH + NEt_3; **(g)** regenerated **4** (via **4** + PPh_3 + CF_3COOH + NEt_3 + [Ru(*p*-cym)Cl_2]$_2$). Residual solvent peak at δ = 7.26 ppm in $CDCl_3$ was taken as reference for all the spectra. The relevant protons in the complex backbone have been labelled (a■, ▲, ♦, and ● on the structure) and shown in the figure. Generation of the decoordinated/recoordinated and protonated/deprotonated species was confirmed by isolation and characterization of the corresponding ruthenium complexes **5**, **6**, and **7** independently as well as by recording ESI-HRMS data in solution (***see section IV and also the experimental section in the main article***).

Table S1 Relevant ^{1}H NMR chemical shift values (in $CDCl_3$) in stimuli-responsive studies with **3**. Residual solvent peak at δ = 7.26 ppm in $CDCl_3$ was taken as reference.

Complex	**H$^{\bullet}$**	**H$^{\bullet}$**	**H$^{\blacksquare}$**	**H$^{\blacklozenge}$**	**H$^{\blacktriangle}$**
3	7.08	7.40	9.04	7.04	8.50
Decoordinated	7.05	a	8.80	7.12	8.18
Protonated	7.18	a	8.69	7.49	8.22
Decoordinated (1st regeneration)	7.04	a	8.85	7.05	8.20
Protonated (1st regeneration)	7.15	7.42	8.73	7.46	8.29
Decoordinated (2nd regeneration)	7.04	a	8.84	7.05	8.20
3 (regenerated after acid-base cycles)	7.07	a	9.04	7.04	8.52
Heterobimetallic	7.07	a	9.11	7.01	8.55

[a] Overlapped with PPh_3

Table S2 Relevant ^{1}H NMR chemical shift values (in $CDCl_3$) in stimuli-responsive studies with **4**. Residual solvent peak at δ = 7.26 ppm in $CDCl_3$ was taken as reference.

Complex	**H$^{\bullet}$**	**H$^{\bullet}$**	**H$^{\blacksquare}$**	**H$^{\blacklozenge}$**	**H$^{\blacktriangle}$**
4	7.05	7.38	9.51	6.91	8.51
Decoordinated 5	7.02	a	9.21	6.96	8.21
Protonated 6	7.13	a	9.13	a	8.21
Decoordinated 5 (regenerated)	7.02	a	9.22	6.96	8.22
Heterobimetallic 7	7.06	a	9.39	6.95	8.45

[a] Overlapped with PPh_3

III. Electrochemical studies:

The electrochemical measurements (cyclic voltammetry, CV and differential pulse voltammetry, DPV) were carried out by a CHI Instrument (CHI 1120B Electrochemical Analyzer) at ambient temperature using a three electrode configuration (working electrode: Pt disk (1 mm diameter); counter electrode: a Pt wire; reference electrode: saturated calomel electrode, SCE). All the samples were prepared in dry acetonitrile and deoxygenated for 5 minutes with nitrogen gas before starting the actual experiments. A 0.1 M solution of $[NBu_4]PF_6$ in dry acetonitrile was used as the supporting electrolyte. Ferrocene ($E_{1/2}$, Fc/Fc^+ = 0.401 volts vs SCE) was used as external calibration standard for all the measurements.

The characterization and determination of the half-wave potentials ($E_{1/2}$) of the corresponding cyclometalated M^n/M^{n+1} redox couples (Ir^{III}/Ir^{IV} and Ru^{II}/Ru^{III}) in the respective complexes was based on correlation with similar studies as reported by Crabtree et al.[S3] The data are shown below in Table S3 and the DPV plots are shown in Figures S24-S25.

Table S3 Half-wave potential ($E_{1/2}$, vs. saturated calomel electrode) values derived from differential pulse voltammetric (DPV) experiments; [complex] ~ 1 mM; supporting electrolyte = $[NBu_4]PF_6$ (0.1 M in MeCN); scan rate = 50 mV/sec; $E_{1/2}$ of Fc/Fc+ = 0.401 V vs SCE (external calibration standard). Complexes were generated *in situ* from **3** and **4** respectively.

Complex	**$E_{1/2}$ (Ir^{III}/Ir^{IV}, Cyclometalated), (Volts, vs SCE)**	**Complex**	**$E_{1/2}$ (Ru^{II}/Ru^{III}, Cyclometalated), (Volts, vs SCE)**
3	0.865	**4**	0.664
Decoordinated (generated via **3** + PPh_3)	0.809	**Decoordinated 5** (generated via **4** + PPh_3)	0.556
Protonated (generated via **3** + PPh_3 + TFA)	0.909	**Protonated 6** (generated via **4** + PPh_3 + TFA)	0.624
Heterobimetallic (generated via **3** + PPh_3 + $[Ru(p\text{-cym})Cl_2]_2$)	0.845	**Heterobimetallic 7** (generated via **4** + PPh_3 + $[IrCp^*Cl_2]_2$)	0.660
$IrCp^*Cl_2(PPh_3)$	1.196	**$Ru(p\text{-cym})Cl_2(PPh_3)$**	1.108

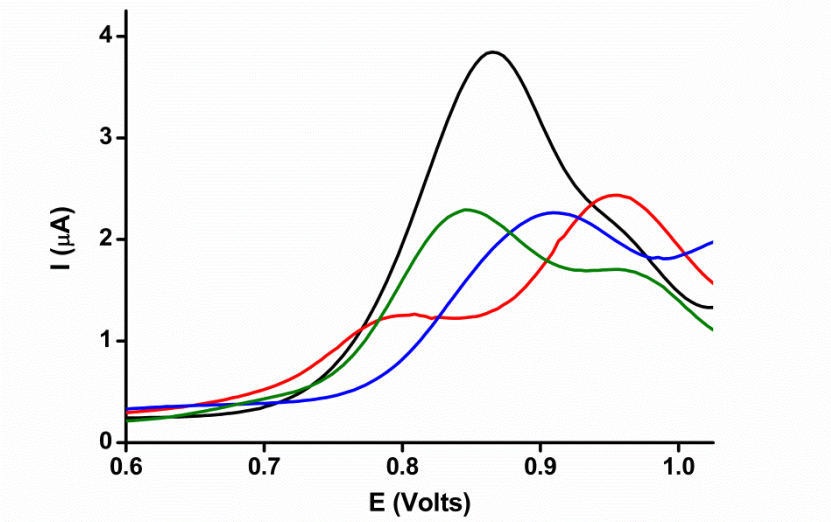

Figure S24 Partial DPV plots of **3** (black)**, Decoordinated** (red)**, Protonated** (blue)**, Heterobimetallic** (green) complexes (see Table S3). The peaks correspond to the Ir^{III}/Ir^{IV} redox couple of "$Ir^{III}(C_{carbene}\text{^}C_{pyridyl})Cp^*Cl$" moiety (based on correlation with similar studies as reported by Crabtree et al.[S3]).
The high-potential region is omitted as these peaks correspond to solvated and other species generated in solution (as reported by Crabtree et al.[S3]).

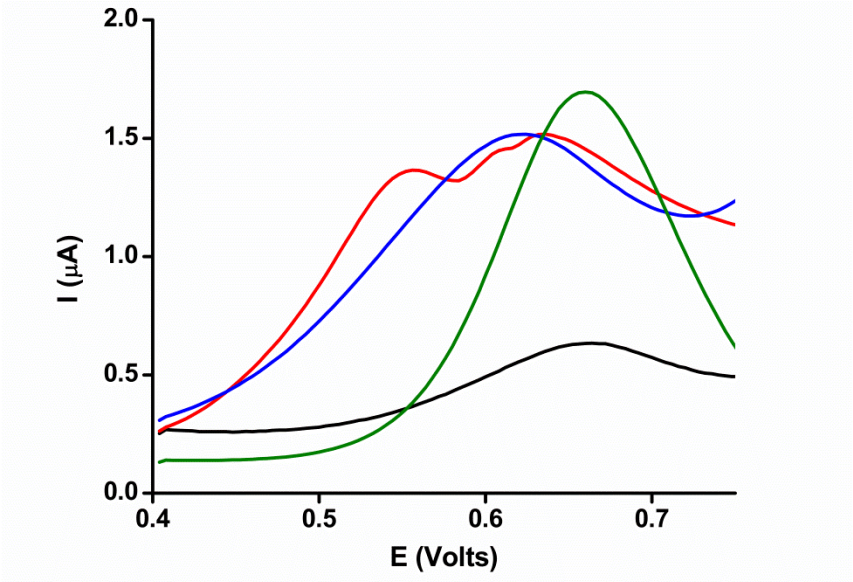

Figure S25 DPV plots of complexes **4** (black)**, Decoordinated 5** (red)**, Protonated 6** (blue)**, Heterobimetallic 7** (green) (see Table S3). The peaks correspond to the Ru^{II}/Ru^{III} redox couple of "$Ru^{II}(C_{carbene}\text{^}C_{pyridyl})(p\text{-cym})Cl$" moiety (based on correlation with similar studies as reported by Crabtree et al.[S3]).
The high-potential region is omitted as these peaks correspond to solvated and other species generated in solution (as reported by Crabtree et al.[S3]).

IV. Additional ESI-MS spectra (of decoordinated, protonated, and heterobimetallic complexes generated in situ):

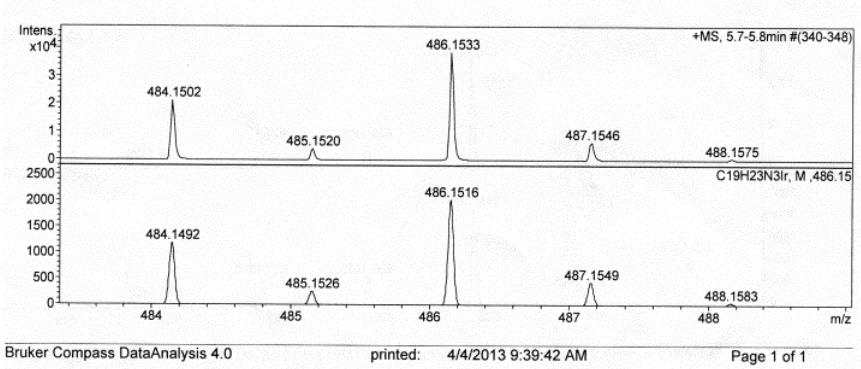

Figure S26 ESI-MS (positive ion mode) spectrum of the decoordinated iridium complex (generated in situ via **3** + PPh_3). HRMS (ESI, positive ion): M^+ = 486.1533 (calculated 486.1516 for $[C_{19}H_{23}N_3Ir]^+$).

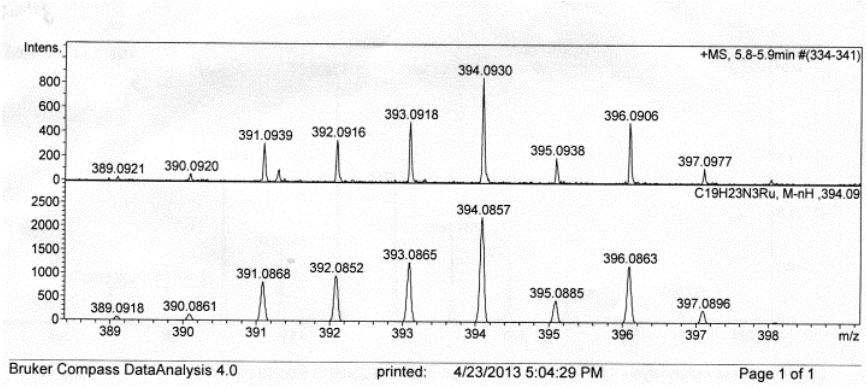

Figure S27 ESI-MS (positive ion mode) spectrum of decoordinated ruthenium complex **5** (generated in situ via **4** + PPh_3). HRMS (ESI, positive ion): M^+ = 394.0930 (calculated 394.0857 for $[C_{19}H_{22}N_3Ru]^+$).

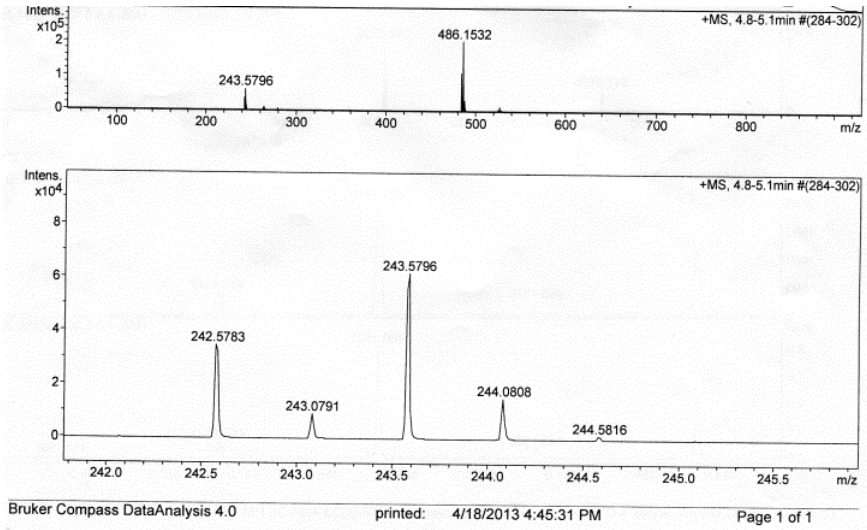

Figure S28 ESI-MS (positive ion mode) spectrum of the protonated iridium complex (generated via **3** + PPh_3 + TFA). HRMS (ESI, positive ion): M^{2+} = 243.5796 (calculated 243.5788 for $[C_{19}H_{23}N_3Ir + H^+]^{2+}$).

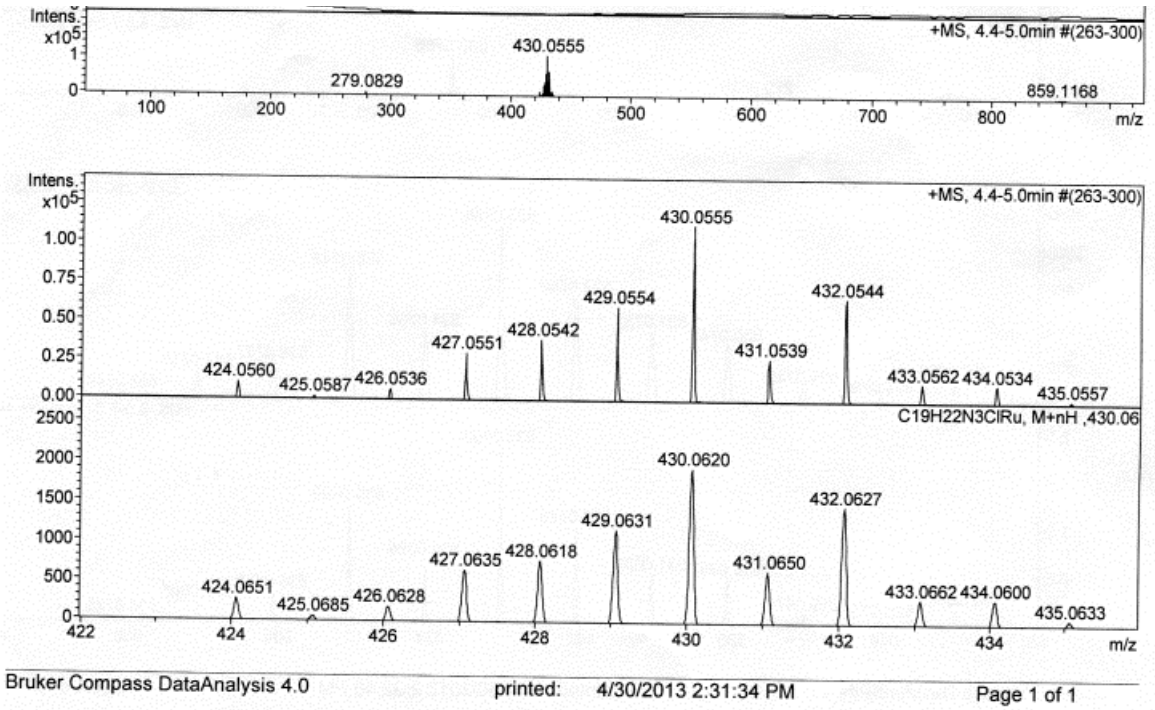

Figure S29 ESI-MS (positive ion mode) spectrum of the protonated ruthenium complex **6** (generated via **4** + PPh_3 + TFA). HRMS (ESI, positive ion): M^+ = 430.0555 (calculated 430.0620 for $[C_{19}H_{22}N_3RuCl + H^+]^+$).

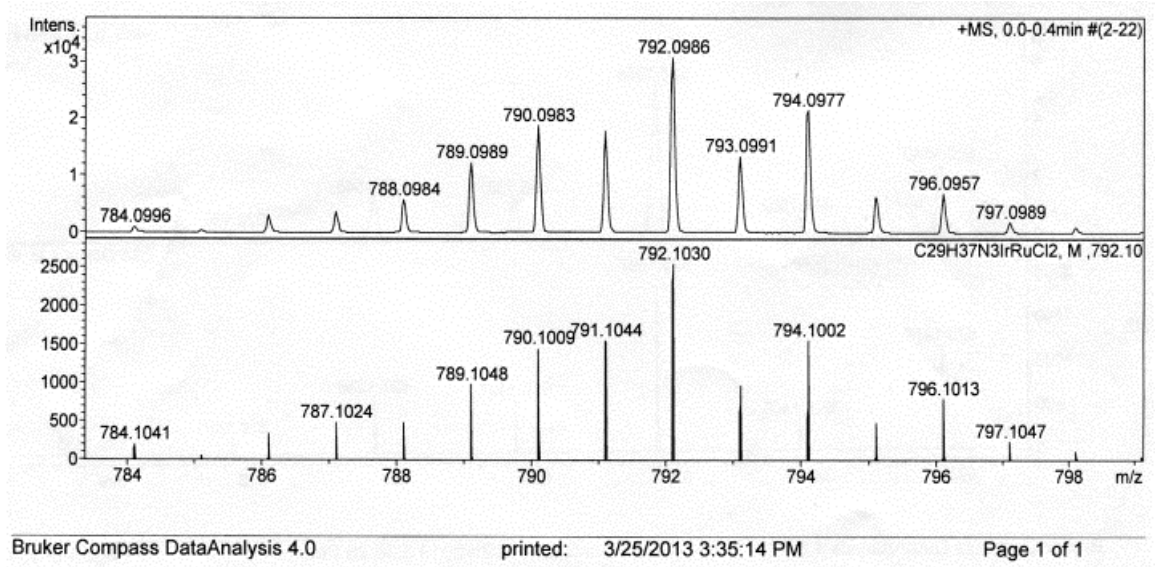

Figure S30 ESI-MS (positive ion mode) spectrum of the heterobimetallic iridium-ruthenium complex (generated via **3** + PPh_3 + $[Ru(p\text{-cym})Cl_2]_2$). HRMS (ESI, positive ion): M^+ = 792.0986 (calculated 792.1030 for $[C_{29}H_{37}N_3Cl_2IrRu]^+$).

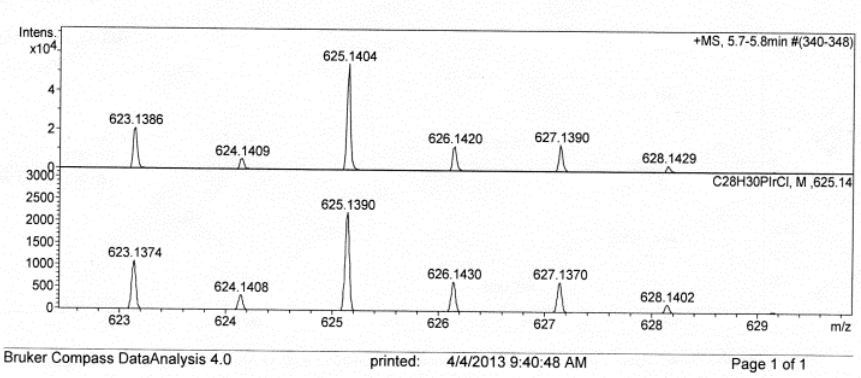

Figure S31 ESI-MS (positive ion mode) spectrum of **[IrCp*Cl$_2$(PPh$_3$)]** (generated *in situ*). HRMS (ESI, positive ion): M^+ = 625.1404 (calculated 625.1390 for $[C_{28}H_{30}PClIr]^+$).

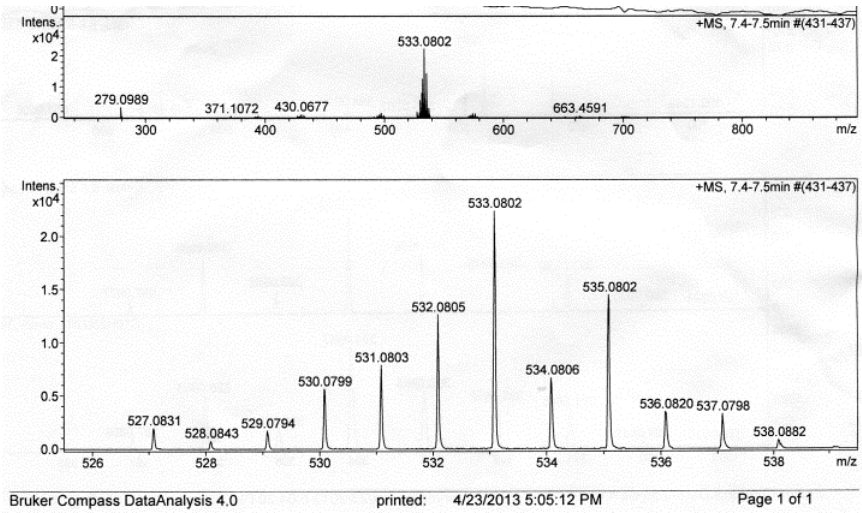

Figure S32 ESI-MS (positive ion mode) spectrum of **[Ru(*p*-cym)Cl$_2$(PPh$_3$)]** (generated *in situ*). HRMS (ESI, positive ion): M^+ = 533.0802 (calculated 533.0771 for $[C_{28}H_{29}PClRu]^+$).

V. X-ray structure analysis:

Single crystals of **3** and **4** suitable for X-ray diffraction studies were grown from solutions in CH_2Cl_2 by solvent diffusion and vapour diffusion of hexane at ~ 4 °C respectively. Data collection were carried out on a Bruker SMART APEX II CCD diffractometer with graphite monochromated Mo Kα (λ = 0.71073 Å) radiation at 140 K. Structures were solved with direct methods using SHELXS-97 and refined with full-matrix least-squares on F^2 using SHELXL-97 [S4]. All non-hydrogen atoms were refined anisotropically. The hydrogen atoms were placed in calculated positions and refined using a riding model with isotropic displacement parameters. During the refinement cycles for the structure of **3**, an attempt of fully anisotropic model for all non-hydrogen atoms led the temperature factors of C(2), C(6), C(12), C(20), C(21), C(22) and C(23) atoms to non-positive definite. DELU and SIMU instructions combined with anisotropic refinement were performed for these carbon atoms but no improvement was achieved. So, isotropic refinement was applied to these 7 carbon atoms to achieve a convenient convergence. The carbon atoms in the pentamethyl cyclopentadienyl ligands were treated

with DELU and SIMU instructions with idealized rigid pentamethyl Cp ring model. In the structure of **4**, hydrogen atoms associated with the two water molecules of crystallisation (O1W and O2W) could not be directly located from difference Fourier maps. Attempts to include these atoms in calculated positions did not improve structural refinements and thus were omitted. The details of crystallographic data and selected bond distances and bond angles for **3** and **4** have been provided in Tables S4a-S4c and S5a-S5c.

Table S4a Crystal data and structure refinement for Complex **3.**

Identification code	JC_TKR_01_32	
Empirical formula	C29 H38 Cl3 Ir2 N3	
Formula weight	919.37	
Temperature	140(2) K	
Wavelength	0.71073 Å	
Crystal system	Orthorhombic	
Space group	Pna21	
Unit cell dimensions	a = 25.9283(6) Å	α = 90°.
	b = 9.0626(2) Å	β = 90°.
	c = 12.5119(3) Å	γ = 90°.
Volume	2940.02(12) $Å^3$	
Z	4	
Density (calculated)	2.077 Mg/m^3	
Absorption coefficient	9.340 mm^{-1}	
F(000)	1752	
Crystal size	0.20 x 0.10 x 0.10 mm^3	
Theta range for data collection	2.26 to 27.53°.	
Index ranges	-32<=h<=33, -11<=k<=11, -15<=l<=15	
Reflections collected	13733	
Independent reflections	6190 [R(int) = 0.0423]	
Completeness to theta = 27.53°	97.5 %	
Max. and min. transmission	0.4552 and 0.2567	
Refinement method	Full-matrix least-squares on F^2	
Data / restraints / parameters	6190 / 114 / 308	
Goodness-of-fit on F^2	1.055	
Final R indices [I>2sigma(I)]	R1 = 0.0471, wR2 = 0.1432	
R indices (all data)	R1 = 0.0493, wR2 = 0.1449	
Absolute structure parameter	0.035(15)	
Largest diff. peak and hole	3.728 and -3.473 $e.Å^{-3}$	

Table S4b Bond lengths [Å] for Complex **3.**

C(1)-N(1)	1.435(16)
C(2)-N(1)	1.315(11)
C(2)-N(2)	1.417(10)
C(2)-Ir(1)	2.0463(4)
C(3)-C(4)	1.336(17)
C(3)-N(1)	1.396(13)
C(4)-N(2)	1.382(14)
C(5)-C(9)	1.374(16)
C(5)-N(2)	1.406(16)
C(5)-C(6)	1.427(12)
C(6)-C(7)	1.334(12)
C(6)-Ir(1)	2.064(4)
C(7)-N(3)	1.404(14)
C(8)-N(3)	1.335(15)
C(8)-C(9)	1.410(17)
C(10)-C(14)	1.436(19)
C(10)-C(11)	1.452(19)
C(10)-C(15)	1.492(19)
C(10)-Ir(1)	2.276(12)
C(11)-C(12)	1.477(18)
C(11)-C(16)	1.537(19)
C(11)-Ir(1)	2.227(11)
C(12)-C(13)	1.469(18)
C(12)-C(17)	1.491(18)
C(12)-Ir(1)	2.174(12)
C(13)-C(14)	1.451(19)
C(13)-C(18)	1.457(18)
C(13)-Ir(1)	2.185(11)
C(14)-C(19)	1.519(18)
C(14)-Ir(1)	2.258(11)
C(20)-C(21)	1.438(17)
C(20)-C(24)	1.452(19)
C(20)-C(25)	1.479(17)
C(20)-Ir(2)	2.133(13)
C(21)-C(22)	1.453(17)
C(21)-C(26)	1.49(2)
C(21)-Ir(2)	2.118(12)

C(22)-C(23)	1.440(19)
C(22)-C(27)	1.511(19)
C(22)-Ir(2)	2.163(14)
C(23)-C(24)	1.449(17)
C(23)-C(28)	1.484(19)
C(23)-Ir(2)	2.137(13)
C(24)-C(29)	1.48(2)
C(24)-Ir(2)	2.165(17)
N(3)-Ir(2)	2.069(11)
Cl(2)-Ir(2)	2.400(3)
Cl(1)-Ir(1)	2.403(3)
Cl(3)-Ir(2)	2.431(3)

Table S4c Bond angles [°] for Complex **3.**

N(1)-C(2)-N(2)	105.5(6)
N(1)-C(2)-Ir(1)	140.5(5)
N(2)-C(2)-Ir(1)	113.9(4)
C(4)-C(3)-N(1)	109.2(10)
C(3)-C(4)-N(2)	106.0(10)
C(9)-C(5)-N(2)	125.7(11)
C(9)-C(5)-C(6)	121.3(11)
N(2)-C(5)-C(6)	113.0(8)
C(7)-C(6)-C(5)	116.7(7)
C(7)-C(6)-Ir(1)	127.8(5)
C(5)-C(6)-Ir(1)	115.6(5)
C(6)-C(7)-N(3)	124.3(9)
N(3)-C(8)-C(9)	122.4(10)
C(5)-C(9)-C(8)	117.8(11)
C(14)-C(10)-C(11)	109.8(12)
C(14)-C(10)-C(15)	125.8(13)
C(11)-C(10)-C(15)	124.3(13)
C(14)-C(10)-Ir(1)	70.8(7)
C(11)-C(10)-Ir(1)	69.4(7)
C(15)-C(10)-Ir(1)	125.6(9)
C(10)-C(11)-C(12)	106.0(11)
C(10)-C(11)-C(16)	125.3(12)
C(12)-C(11)-C(16)	128.4(12)
C(10)-C(11)-Ir(1)	73.0(7)
C(12)-C(11)-Ir(1)	68.4(6)

C(16)-C(11)-Ir(1)	128.0(8)
C(13)-C(12)-C(11)	108.5(11)
C(13)-C(12)-C(17)	126.6(11)
C(11)-C(12)-C(17)	124.7(11)
C(13)-C(12)-Ir(1)	70.7(7)
C(11)-C(12)-Ir(1)	72.4(7)
C(17)-C(12)-Ir(1)	126.9(8)
C(14)-C(13)-C(18)	126.6(12)
C(14)-C(13)-C(12)	107.1(11)
C(18)-C(13)-C(12)	125.9(13)
C(14)-C(13)-Ir(1)	73.7(7)
C(18)-C(13)-Ir(1)	127.0(8)
C(12)-C(13)-Ir(1)	69.9(6)
C(10)-C(14)-C(13)	108.5(11)
C(10)-C(14)-C(19)	125.0(13)
C(13)-C(14)-C(19)	125.6(13)
C(10)-C(14)-Ir(1)	72.2(7)
C(13)-C(14)-Ir(1)	68.3(6)
C(19)-C(14)-Ir(1)	133.8(9)
C(21)-C(20)-C(24)	107.8(10)
C(21)-C(20)-C(25)	124.9(13)
C(24)-C(20)-C(25)	127.3(13)
C(21)-C(20)-Ir(2)	69.7(7)
C(24)-C(20)-Ir(2)	71.4(8)
C(25)-C(20)-Ir(2)	126.5(10)
C(20)-C(21)-C(22)	108.4(11)
C(20)-C(21)-C(26)	126.5(11)
C(22)-C(21)-C(26)	124.7(12)
C(20)-C(21)-Ir(2)	70.8(7)
C(22)-C(21)-Ir(2)	71.8(7)
C(26)-C(21)-Ir(2)	129.3(10)
C(23)-C(22)-C(21)	107.7(11)
C(23)-C(22)-C(27)	126.1(14)
C(21)-C(22)-C(27)	126.2(14)
C(23)-C(22)-Ir(2)	69.5(7)
C(21)-C(22)-Ir(2)	68.5(7)
C(27)-C(22)-Ir(2)	127.2(10)
C(22)-C(23)-C(24)	108.2(11)
C(22)-C(23)-C(28)	124.8(13)
C(24)-C(23)-C(28)	126.8(14)

C(22)-C(23)-Ir(2)	71.4(8)
C(24)-C(23)-Ir(2)	71.4(9)
C(28)-C(23)-Ir(2)	127.2(10)
C(23)-C(24)-C(20)	107.8(12)
C(23)-C(24)-C(29)	125.9(13)
C(20)-C(24)-C(29)	126.3(12)
C(23)-C(24)-Ir(2)	69.3(8)
C(20)-C(24)-Ir(2)	69.1(9)
C(29)-C(24)-Ir(2)	125.6(12)
C(2)-N(1)-C(3)	109.9(9)
C(2)-N(1)-C(1)	125.1(9)
C(3)-N(1)-C(1)	124.8(11)
C(4)-N(2)-C(5)	132.6(10)
C(4)-N(2)-C(2)	109.4(8)
C(5)-N(2)-C(2)	117.8(8)
C(8)-N(3)-C(7)	117.5(11)
C(8)-N(3)-Ir(2)	124.3(8)
C(7)-N(3)-Ir(2)	117.7(8)
C(2)-Ir(1)-C(6)	79.47(9)
C(2)-Ir(1)-C(12)	125.3(4)
C(6)-Ir(1)-C(12)	95.8(4)
C(2)-Ir(1)-C(13)	99.6(3)
C(6)-Ir(1)-C(13)	123.5(4)
C(12)-Ir(1)-C(13)	39.4(5)
C(2)-Ir(1)-C(11)	164.0(4)
C(6)-Ir(1)-C(11)	103.2(3)
C(12)-Ir(1)-C(11)	39.2(5)
C(13)-Ir(1)-C(11)	65.6(5)
C(2)-Ir(1)-C(14)	109.0(3)
C(6)-Ir(1)-C(14)	159.5(4)
C(12)-Ir(1)-C(14)	64.0(5)
C(13)-Ir(1)-C(14)	38.1(5)
C(11)-Ir(1)-C(14)	63.6(5)
C(2)-Ir(1)-C(10)	142.4(4)
C(6)-Ir(1)-C(10)	138.1(4)
C(12)-Ir(1)-C(10)	63.4(5)
C(13)-Ir(1)-C(10)	63.3(5)
C(11)-Ir(1)-C(10)	37.6(5)
C(14)-Ir(1)-C(10)	36.9(5)
C(2)-Ir(1)-Cl(1)	91.6(2)

C(6)-Ir(1)-Cl(1)	85.9(2)
C(12)-Ir(1)-Cl(1)	142.9(3)
C(13)-Ir(1)-Cl(1)	149.9(4)
C(11)-Ir(1)-Cl(1)	104.2(3)
C(14)-Ir(1)-Cl(1)	111.8(4)
C(10)-Ir(1)-Cl(1)	91.0(3)
N(3)-Ir(2)-C(21)	153.3(4)
N(3)-Ir(2)-C(20)	113.7(4)
C(21)-Ir(2)-C(20)	39.5(5)
N(3)-Ir(2)-C(23)	107.1(5)
C(21)-Ir(2)-C(23)	66.6(5)
C(20)-Ir(2)-C(23)	66.6(5)
N(3)-Ir(2)-C(22)	145.4(5)
C(21)-Ir(2)-C(22)	39.7(5)
C(20)-Ir(2)-C(22)	66.1(5)
C(23)-Ir(2)-C(22)	39.1(5)
N(3)-Ir(2)-C(24)	92.3(5)
C(21)-Ir(2)-C(24)	66.1(5)
C(20)-Ir(2)-C(24)	39.5(5)
C(23)-Ir(2)-C(24)	39.4(5)
C(22)-Ir(2)-C(24)	65.4(5)
N(3)-Ir(2)-Cl(2)	88.5(3)
C(21)-Ir(2)-Cl(2)	93.8(3)
C(20)-Ir(2)-Cl(2)	96.0(4)
C(23)-Ir(2)-Cl(2)	160.0(4)
C(22)-Ir(2)-Cl(2)	126.1(4)
C(24)-Ir(2)-Cl(2)	130.2(3)
N(3)-Ir(2)-Cl(3)	85.4(3)
C(21)-Ir(2)-Cl(3)	121.2(3)
C(20)-Ir(2)-Cl(3)	159.7(4)
C(23)-Ir(2)-Cl(3)	102.4(3)
C(22)-Ir(2)-Cl(3)	94.4(4)
C(24)-Ir(2)-Cl(3)	138.7(3)
Cl(2)-Ir(2)-Cl(3)	90.98(11)

Table S5a Crystal data and structure refinement for Complex **4.**

Identification code	JC_MM_58_0m
Empirical formula	C29 H36 Cl3 N3 O2 Ru2
Formula weight	767.10

Temperature	140(2) K	
Wavelength	0.71073 Å	
Crystal system	Monoclinic	
Space group	P2(1)/n	
Unit cell dimensions	a = 11.7528(4) Å	α = 90°.
	b = 18.8583(7) Å	β = 93.097(2)°.
	c = 13.8022(5) Å	γ = 90°.
Volume	3054.62(19) $Å^3$	
Z	4	
Density (calculated)	1.668 Mg/m^3	
Absorption coefficient	1.282 mm^{-1}	
F(000)	1544	
Crystal size	0.20 x 0.20 x 0.15 mm^3	
Theta range for data collection	1.83 to 27.57°.	
Index ranges	-15<=h<=15, -24<=k<=24, -17<=l<=17	
Reflections collected	48958	
Independent reflections	7049 [R(int) = 0.0458]	
Completeness to theta = 27.57°	99.8 %	
Max. and min. transmission	0.8309 and 0.7835	
Refinement method	Full-matrix least-squares on F^2	
Data / restraints / parameters	7049 / 0 / 352	
Goodness-of-fit on F^2	1.055	
Final R indices [I>2sigma(I)]	R1 = 0.0443, wR2 = 0.0974	
R indices (all data)	R1 = 0.0598, wR2 = 0.1030	
Largest diff. peak and hole	1.072 and -0.679 $e.Å^{-3}$	

Table S5b Bond lengths [Å] for Complex **4.**

Ru(1)-C(2)	2.016(4)
Ru(1)-C(6)	2.067(4)
Ru(1)-C(10)	2.150(4)
Ru(1)-C(15)	2.172(4)
Ru(1)-C(14)	2.217(4)
Ru(1)-C(13)	2.254(4)
Ru(1)-C(11)	2.289(4)
Ru(1)-C(12)	2.333(4)
Ru(1)-Cl(1)	2.4357(12)
Ru(2)-N(3)	2.143(3)

Ru(2)-C(24)	2.167(4)
Ru(2)-C(23)	2.168(4)
Ru(2)-C(20)	2.171(5)
Ru(2)-C(21)	2.187(4)
Ru(2)-C(25)	2.196(4)
Ru(2)-C(22)	2.216(4)
Ru(2)-Cl(2)	2.4104(13)
Ru(2)-Cl(3)	2.4210(13)
N(2)-C(2)	1.376(5)
N(2)-C(4)	1.390(5)
N(2)-C(5)	1.412(5)
N(1)-C(2)	1.348(5)
N(1)-C(3)	1.398(5)
N(1)-C(1)	1.455(5)
C(8)-N(3)	1.337(5)
C(8)-C(9)	1.387(6)
C(6)-C(7)	1.383(5)
C(6)-C(5)	1.402(5)
N(3)-C(7)	1.361(5)
C(5)-C(9)	1.372(6)
C(12)-C(11)	1.380(7)
C(12)-C(13)	1.432(6)
C(12)-C(16)	1.501(7)
C(10)-C(11)	1.410(6)
C(10)-C(15)	1.421(6)
C(29)-C(27)	1.529(7)
C(4)-C(3)	1.333(6)
C(23)-C(24)	1.396(6)
C(23)-C(22)	1.430(6)
C(20)-C(25)	1.401(6)
C(20)-C(21)	1.424(7)
C(24)-C(25)	1.427(6)
C(15)-C(14)	1.432(6)
C(15)-C(17)	1.505(6)
C(17)-C(19)	1.530(7)
C(17)-C(18)	1.537(7)
C(14)-C(13)	1.380(6)
C(21)-C(22)	1.394(7)
C(27)-C(28)	1.504(7)
C(27)-C(25)	1.518(6)

C(26)-C(22)	1.490(6)

Table S5c Bond angles [°] for Complex **4.**

C(2)-Ru(1)-C(6)	76.76(16)
C(2)-Ru(1)-C(10)	92.12(16)
C(6)-Ru(1)-C(10)	120.57(16)
C(2)-Ru(1)-C(15)	111.12(16)
C(6)-Ru(1)-C(15)	91.72(16)
C(10)-Ru(1)-C(15)	38.39(16)
C(2)-Ru(1)-C(14)	147.77(16)
C(6)-Ru(1)-C(14)	92.15(15)
C(10)-Ru(1)-C(14)	67.36(16)
C(15)-Ru(1)-C(14)	38.08(16)
C(2)-Ru(1)-C(13)	165.71(16)
C(6)-Ru(1)-C(13)	117.12(16)
C(10)-Ru(1)-C(13)	78.03(17)
C(15)-Ru(1)-C(13)	67.14(16)
C(14)-Ru(1)-C(13)	35.93(15)
C(2)-Ru(1)-C(11)	101.79(16)
C(6)-Ru(1)-C(11)	157.35(16)
C(10)-Ru(1)-C(11)	36.87(17)
C(15)-Ru(1)-C(11)	67.44(16)
C(14)-Ru(1)-C(11)	77.04(16)
C(13)-Ru(1)-C(11)	64.16(16)
C(2)-Ru(1)-C(12)	129.88(16)
C(6)-Ru(1)-C(12)	153.36(16)
C(10)-Ru(1)-C(12)	65.26(17)
C(15)-Ru(1)-C(12)	79.04(16)
C(14)-Ru(1)-C(12)	65.20(16)
C(13)-Ru(1)-C(12)	36.32(16)
C(11)-Ru(1)-C(12)	34.73(16)
C(2)-Ru(1)-Cl(1)	90.00(12)
C(6)-Ru(1)-Cl(1)	89.27(11)
C(10)-Ru(1)-Cl(1)	149.74(13)
C(15)-Ru(1)-Cl(1)	158.51(12)
C(14)-Ru(1)-Cl(1)	120.44(12)
C(13)-Ru(1)-Cl(1)	93.40(12)
C(11)-Ru(1)-Cl(1)	113.38(13)
C(12)-Ru(1)-Cl(1)	90.60(12)

N(3)-Ru(2)-C(24)	91.49(14)
N(3)-Ru(2)-C(23)	117.09(15)
C(24)-Ru(2)-C(23)	37.58(16)
N(3)-Ru(2)-C(20)	118.72(15)
C(24)-Ru(2)-C(20)	67.87(17)
C(23)-Ru(2)-C(20)	80.66(18)
N(3)-Ru(2)-C(21)	156.83(16)
C(24)-Ru(2)-C(21)	79.93(17)
C(23)-Ru(2)-C(21)	67.58(17)
C(20)-Ru(2)-C(21)	38.13(17)
N(3)-Ru(2)-C(25)	91.78(14)
C(24)-Ru(2)-C(25)	38.18(16)
C(23)-Ru(2)-C(25)	68.69(17)
C(20)-Ru(2)-C(25)	37.43(17)
C(21)-Ru(2)-C(25)	68.18(17)
N(3)-Ru(2)-C(22)	154.98(15)
C(24)-Ru(2)-C(22)	68.09(16)
C(23)-Ru(2)-C(22)	38.05(16)
C(20)-Ru(2)-C(22)	68.09(17)
C(21)-Ru(2)-C(22)	36.92(17)
C(25)-Ru(2)-C(22)	81.04(16)
N(3)-Ru(2)-Cl(2)	84.64(10)
C(24)-Ru(2)-Cl(2)	116.59(13)
C(23)-Ru(2)-Cl(2)	90.56(13)
C(20)-Ru(2)-Cl(2)	156.57(13)
C(21)-Ru(2)-Cl(2)	118.47(13)
C(25)-Ru(2)-Cl(2)	154.56(12)
C(22)-Ru(2)-Cl(2)	91.64(13)
N(3)-Ru(2)-Cl(3)	89.13(9)
C(24)-Ru(2)-Cl(3)	156.36(13)
C(23)-Ru(2)-Cl(3)	153.33(13)
C(20)-Ru(2)-Cl(3)	91.22(14)
C(21)-Ru(2)-Cl(3)	90.38(13)
C(25)-Ru(2)-Cl(3)	118.19(12)
C(22)-Ru(2)-Cl(3)	115.43(12)
Cl(2)-Ru(2)-Cl(3)	87.00(6)
C(2)-N(2)-C(4)	111.6(3)
C(2)-N(2)-C(5)	115.4(3)
C(4)-N(2)-C(5)	132.9(4)
C(2)-N(1)-C(3)	110.4(3)

C(2)-N(1)-C(1)	124.7(4)
C(3)-N(1)-C(1)	124.9(4)
N(3)-C(8)-C(9)	122.2(4)
C(7)-C(6)-C(5)	114.3(3)
C(7)-C(6)-Ru(1)	128.7(3)
C(5)-C(6)-Ru(1)	117.0(3)
C(8)-N(3)-C(7)	118.1(3)
C(8)-N(3)-Ru(2)	123.6(3)
C(7)-N(3)-Ru(2)	118.2(3)
C(9)-C(5)-C(6)	122.9(4)
C(9)-C(5)-N(2)	124.8(4)
C(6)-C(5)-N(2)	112.3(3)
C(5)-C(9)-C(8)	117.7(4)
C(11)-C(12)-C(13)	118.2(4)
C(11)-C(12)-C(16)	122.1(4)
C(13)-C(12)-C(16)	119.7(4)
C(11)-C(12)-Ru(1)	70.9(2)
C(13)-C(12)-Ru(1)	68.8(2)
C(16)-C(12)-Ru(1)	131.1(3)
C(11)-C(10)-C(15)	122.2(4)
C(11)-C(10)-Ru(1)	76.9(3)
C(15)-C(10)-Ru(1)	71.7(2)
C(3)-C(4)-N(2)	105.6(4)
C(24)-C(23)-C(22)	120.5(4)
C(24)-C(23)-Ru(2)	71.2(2)
C(22)-C(23)-Ru(2)	72.8(2)
N(1)-C(2)-N(2)	104.1(3)
N(1)-C(2)-Ru(1)	137.7(3)
N(2)-C(2)-Ru(1)	118.1(3)
C(12)-C(11)-C(10)	120.5(4)
C(12)-C(11)-Ru(1)	74.4(3)
C(10)-C(11)-Ru(1)	66.2(2)
C(25)-C(20)-C(21)	120.8(4)
C(25)-C(20)-Ru(2)	72.3(3)
C(21)-C(20)-Ru(2)	71.5(3)
C(23)-C(24)-C(25)	121.4(4)
C(23)-C(24)-Ru(2)	71.2(2)
C(25)-C(24)-Ru(2)	72.0(2)
C(10)-C(15)-C(14)	116.2(4)
C(10)-C(15)-C(17)	124.6(4)

C(14)-C(15)-C(17)	119.2(4)
C(10)-C(15)-Ru(1)	69.9(2)
C(14)-C(15)-Ru(1)	72.6(2)
C(17)-C(15)-Ru(1)	129.5(3)
C(4)-C(3)-N(1)	108.4(4)
C(15)-C(17)-C(19)	113.6(4)
C(15)-C(17)-C(18)	108.3(4)
C(19)-C(17)-C(18)	111.3(4)
N(3)-C(7)-C(6)	124.7(4)
C(13)-C(14)-C(15)	121.1(4)
C(13)-C(14)-Ru(1)	73.5(2)
C(15)-C(14)-Ru(1)	69.3(2)
C(22)-C(21)-C(20)	121.3(4)
C(22)-C(21)-Ru(2)	72.7(3)
C(20)-C(21)-Ru(2)	70.3(2)
C(28)-C(27)-C(25)	113.6(4)
C(28)-C(27)-C(29)	111.0(5)
C(25)-C(27)-C(29)	107.6(4)
C(14)-C(13)-C(12)	121.5(4)
C(14)-C(13)-Ru(1)	70.6(2)
C(12)-C(13)-Ru(1)	74.9(2)
C(21)-C(22)-C(23)	118.1(4)
C(21)-C(22)-C(26)	121.5(4)
C(23)-C(22)-C(26)	120.3(4)
C(21)-C(22)-Ru(2)	70.4(2)
C(23)-C(22)-Ru(2)	69.2(2)
C(26)-C(22)-Ru(2)	129.3(3)
C(20)-C(25)-C(24)	117.8(4)
C(20)-C(25)-C(27)	123.9(4)
C(24)-C(25)-C(27)	118.3(4)
C(20)-C(25)-Ru(2)	70.3(3)
C(24)-C(25)-Ru(2)	69.8(2)
C(27)-C(25)-Ru(2)	129.7(3)

VI. References:

S1 J. W. Kang, K. Moseley and P. M. Maitlis, *J. Am. Chem. Soc.*, 1969, **91**, 5970.

S2 E. Hodson and S. J. Simpson, *Polyhedron,* 2004, **23**, 2695.

S3 T. P. Brewster, J. D. Blakemore, N. D. Schley, C. D. Incarvito, N. Hazari, G. W. Brudvig and R. H. Crabtree, *Organometallics*, 2011, **30**, 965.

S4 G. M. Sheldrick, *Acta Crystallogr., Sect. A,* 2008, **64**, 112.